

A COMBINED EXPERIMENTAL AND COMPUTATIONAL INVESTIGATION ON THE SYNTHESIS OF ACETALDEHYDE [CH₃CHO(*X*¹*A*')] IN INTERSTELLAR ICES

CHRIS J. BENNETT,¹ COREY S. JAMIESON,¹ YOSHIHIRO OSAMURA,² AND RALF I. KAISER^{1,3,4}

Received 2004 July 21; accepted 2005 January 20

ABSTRACT

The synthetic routes to form acetaldehyde [CH₃CHO(*X*¹*A*')] in extraterrestrial ices were investigated experimentally in a contamination-free ultrahigh vacuum scattering machine. Binary ice mixtures of carbon monoxide [CO(*X*¹ Σ^+)] and methane [CH₄(*X*¹*A*₁)] were condensed at 10 K onto a silver monocrystal and irradiated with 5 keV electrons to mimic the electronic energy transfer processes initiated by MeV cosmic-ray particle-induced δ -electrons in the “ultrack” of MeV ion trajectories; the carbon monoxide–methane ices served as model compounds to simulate neighboring CO–CH₄ molecules in astrophysical ices, as present in cold molecular clouds and in cometary matter. Upon completion of the high-energy processing, the ice samples sublimed during the heating phase to 293 K, thus releasing the remaining reactants as well as the newly formed molecules into the gas phase. The experiment was monitored on line and in situ via a Fourier transform infrared (FTIR) spectrometer in absorption-reflection-absorption mode (solid state) and a quadrupole mass spectrometer (gas phase). Our investigations were combined with electronic structure calculations. At 10 K, the primary reaction step involved the cleavage of the carbon-hydrogen bond of the methane molecule via an electronic energy transfer process from the impinging electron to the methane molecule to form a methyl radical [CH₃(*X*²*A*₂'')] plus a hydrogen atom [H(²*S*_{1/2})]. The H atom contains the excess energy in the form of translational motion; suprathreshold hydrogen atoms can add to the carbon-oxygen triple bond of the carbon monoxide molecule, overcoming the entrance barrier, to yield the formyl radical [HCO(*X*²*A*')]. Depending on the reactant geometry inside the matrix cage, the formyl radical recombined barrierlessly with the *neighboring* methyl radical *inside* the ices at 10 K. Upon warming of the ice sample, the acetaldehyde molecules sublime into the gas phase. This process mimics the sublimation of molecules from the grain mantles into the gas phase upon the transition of the molecular cloud to the hot molecular core phase. This mechanism to form acetaldehyde inside interstellar ices (cold molecular clouds; 10 K) upon high-energy processing, followed by a radical-radical recombination and sublimation in the hot core phase (molecular cores; few 100 K), presents a compelling route to account for high fractional abundances of acetaldehyde of a few times 10^{−9} toward star-forming regions, as compared to abundances of only some 10^{−10} in the cold cloud TMC-1, where solely gas-phase reactions are supposed to synthesize acetaldehyde.

Subject headings: astrobiology — astrochemistry — comets: general — ISM: molecules — methods: laboratory — molecular processes

1. INTRODUCTION

Untangling the synthetic routes to form complex organic molecules in the interstellar medium presents an important means to an understanding of the chemical evolution of cold molecular clouds, hot molecular cores, and star-forming regions (Millar & Hatchell 1998; Minh & van Dishoeck 2000). Since the transition from the molecular cloud to the hot core phase depends strongly on the molecular composition, it is of paramount importance to unravel the basic physical and chemical processes of how molecules are formed in these environments. A detailed understanding of the synthesis of acetaldehyde [CH₃CHO(*X*¹*A*')] is of particular pertinence to testing chemical models of molecular clouds and hot cores, as this molecule plays an important role in astrobiology (Hjalmarson et al. 2001). So far, acetaldehyde has been observed in the gas phase in three types of interstellar environments: (1) in translucent clouds such as CB 17, CB 24, and CB 228 (Turner et al. 1999); (2) in cold molecular clouds such as the Taurus molecular cloud (TMC-1) and L134N (Matthews

et al. 1985; Turner et al. 1999; Minh & van Dishoeck 2000); and (3) toward hot cores and star-forming regions such as Sgr B2, NGC 6334F, and the Orion compact ridge (Fourikis et al. 1974; Bell et al. 1983; Turner 1991; Ziurys & McGonagle 1993; Nummelin et al. 1998; Ikeda et al. 2001; Charnley 2004). A recent survey carried out by Gibb et al. (2004) using the *Infrared Space Observatory* (ISO) also assigned a 7.414 μ m (1438 cm^{−1}) absorption feature to acetaldehyde found in interstellar ices toward 12 of 23 infrared sources studied (mostly young stellar objects [YSOs] surrounded by icy grains), including W33A and AFGL 7009S. In addition, the presence of acetaldehyde in comets, such as C/1995 O1 (Hale-Bopp), has recently been confirmed (Crovisier et al. 2004).

Despite the important role of acetaldehyde as an evolutionary tracer in astronomy, astrochemistry, and astrobiology, no conclusive evidence has been given so far on its formation processes. The majority of mechanistic information on potential synthetic routes has been derived from chemical reaction networks that actually model the formation of complex organic molecules in interstellar environments. Models of pure gas-phase chemistry in cold molecular clouds focus on ion-molecule reactions to form C₂H₅O⁺ ions via radiative associations, followed by a dissociative recombination to yield the desired acetaldehyde molecule (Fairley et al. 1996; El-Nawawy et al. 1997). Assuming a standard cosmic-ray ionization rate of 1 \times 10^{−17} s^{−1}, these models reproduce nicely the observed fractional abundances of acetaldehyde

¹ Department of Chemistry, University of Hawai'i at Manoa, Honolulu, HI 96822.

² Department of Chemistry, Rikkyo University, 3-34-1 Nishi-ikebukuro, Tokyo 171-8501, Japan.

³ Department of Physics and Astronomy, Open University, Milton Keynes MK7 6AA, UK.

⁴ Corresponding author; kaiser@gold.chem.hawaii.edu.

of $(3-6) \times 10^{-10}$ relative to molecular hydrogen in cold clouds like TMC-1.

However, ion-molecule reaction networks were not able to reproduce fractional abundances of acetaldehyde in hot cores and star-forming regions, where predicted abundances are only 5×10^{-12} (Millar et al. 1991; Dickens et al. 1997). These data underestimate those obtained from Nobeyama Radio Observatory (NRO) and Swedish-ESO Submillimetre Telescope (SEST) observations of Sgr B2 by a factor of at least 1000 (Nummelin et al. 1998). Therefore, pure gas-phase reaction networks failed to model the observed fractional abundances up to a few times 10^{-9} . Compared to cold molecular clouds, hot core regions hold higher temperatures of up to 200 K, compared to 10 K in molecular cloud environments. In hot cores, the enhanced temperature triggers a sublimation of molecules from the icy grains into the gas phase. To explain the increased abundances of acetaldehyde in hot cores compared to cold molecular clouds, Millar et al. (1997) simulated these sublimation processes and injected molecules from the solid state into the gas phase to enhance the production of acetaldehyde via gas-phase ion-molecule reactions. Nevertheless, these models could not reproduce the abundances of complex molecules such as acetaldehyde, dimethylether (CH_3OCH_3), and methanol (CH_3OH) simultaneously; depending on the physical and chemical conditions in the models, molecular abundances are a factor of 100 too high or too low.

Alternative scenarios propose the formation of acetaldehyde via grain-surface reactions of hydrogen, carbon, and oxygen atoms in cold molecular clouds through radical-radical reactions on interstellar grains at 10 K (Tielens & Hagen 1982) and then liberation into the gas phase via sublimation in hot cores when the surrounding matter is heated by the embedded protostar (Millar & Hatchel 1998). However, even this refined model could not fit observed abundances of acetaldehyde. Very recently, Ruffle & Herbst (2001) incorporated effects of surface photochemistry in quiescent dense cores into a combined gas-phase and grain-surface model. Although this approach did not investigate the formation of acetaldehyde explicitly, the authors concluded that the inclusion of these processes only slightly increases molecular abundances and that grain-surface photochemistry has only a minor role because of the small ultraviolet photon flux and the mitigating effect of hydrogen atoms. Here atomic hydrogen migrates more rapidly than any other atom or radical on the 10 K grain surfaces, thus saturating the free valences of radical intermediates and inhibiting the formation of complex organic molecules.

These considerations make it exceptionally clear that neither gas-phase ion-molecule reactions nor grain-surface processes can explain the enhanced abundances of acetaldehyde in star-forming regions of a few times 10^{-9} ; key production routes to form acetaldehyde are still missing. The postulate that the material inside the nanometer-thick ice mantles of grains in molecular clouds—predominantly water (H_2O), methanol (CH_3OH), carbon monoxide (CO), carbon dioxide (CO_2), and minor components such as ammonia (NH_3), formaldehyde (H_2CO), hydrogen cyanide (HCN), carbonyl sulfide (OCS), and methane (CH_4) (Ehrenfreund & Schutte 2000; Gibb et al. 2000, 2004; Fraser et al. 2002)—is chemically inert at 10 K presents the crucial drawback. This assumption limits the validity even of sophisticated grain-surface models dramatically, since the chemical evolution of interstellar and cometary ices by bombardment with broadband ultraviolet (UV) photons (Gerakines et al. 1996; Allamandola et al. 1999; Dartois et al. 1999; Schutte 1999; Bernstein et al. 2002; Muñoz Caro & Schutte 2003) and MeV cosmic rays and keV solar wind particles is well established (Johnson 1990, 1996; Brucato et al. 1997; Kaiser & Roessler

1997, 1998; Smith 1997; Lecluse et al. 1998; Strazzulla & Palumbo 1998; Hudson & Moore 1999; Kaiser et al. 1999; Palumbo et al. 1999, 2000; Bennett et al. 2004; Gerakines et al. 2004). Therefore, pristine ice mantles can be processed chemically by the high-energy cosmic radiation field. Once complex molecules such as acetaldehyde have been formed *inside* ices, the inherent temperature increase from 10 to up to 200 K that goes along with the transition from the cold molecular cloud to the hot core phase could lead to a sublimation of the newly formed molecules into the gas phase. If the assignment by Gibb et al. (2004) of acetaldehyde being present in icy grains is correct, then this accentuates the likelihood of a large proportion of the acetaldehyde observed in the gas phase that can be explained by sublimation from ices. However, the question as to the formation mechanism of acetaldehyde inside these grains presents a new problem to be answered, and is likely to come from studying the processing of simpler precursor molecules already firmly established as present within these grains.

Despite the importance of high-energy particle-induced chemical alterations of pristine extraterrestrial ices to form new molecules, these processes have never been included comprehensively into astrophysical reaction networks modeling the formation of acetaldehyde. Therefore, novel laboratory experiments on the formation of acetaldehyde in extraterrestrial ices are clearly desired. The prime objective of this project is to investigate experimentally the formation of acetaldehyde in interstellar ices via charged particles of the cosmic-ray radiation field and to carry out simulation experiments under well-defined physicochemical conditions that mimic the high-energy particle component, the temperatures, and the chemical composition of cold molecular clouds and hot cores in an ultrahigh vacuum scattering machine. These experiments are augmented by electronic structure calculations to investigate the reactivity of radiolytically produced radicals and reactive intermediates involved in the formation of acetaldehyde theoretically. Both sets of data will help to provide synthetic routes to synthesize acetaldehyde in cold molecular clouds, hot cores, and also in cometary ices.

2. SIMULATION CONDITIONS

2.1. High-Energy Components

Simulation experiments of the formation of complex organic molecules in extraterrestrial ices can never mimic the complexity of interstellar environments, i.e., the wide energy range of the high-energy photons and charged particles (and their chemical composition), the temperatures, and the composition of ice targets itself, simultaneously. Therefore, an understanding of these processes must first be based on simulation experiments involving relatively simple model systems under controlled conditions, before these studies are extended to more complex systems. First and foremost, it is essential to select the appropriate class of high-energy radiation, i.e., UV photons versus charged cosmic-ray particles, which interact with the astrophysically important ice mixtures. Here, a cosmic-ray-induced internal ultraviolet radiation ($\lambda < 13.6$ eV) is present even in the deep interior of dense clouds, holding a fluence $\phi = 10^3$ photons $\text{cm}^{-2} \text{s}^{-1}$ (Prasad & Tarafdar 1983). The particle component consists of about 98% protons (p , H^+) and 2% helium nuclei (α -particles, He^{2+}) and has a distribution maximum at about 10 MeV with $\phi = 10$ particles $\text{cm}^{-2} \text{s}^{-1}$ (Strazzulla & Johnson 1991). Although the fluence of the UV field is 2 orders of magnitude larger than the cosmic-ray particle fluence, we would like to recall that UV photons are absorbed within the first tens of nanometers of the ice via single-quantum processes (i.e., interaction with only one

molecule per photon); on the other hand, MeV cosmic-ray particles can penetrate the ice layer and induce collision cascades and generate up to 10² suprathreshold particles within the surrounding ice matrix (by suprathreshold, we are referring to particles that, because of the excess energy they have gained from the impinging radiation, are not in thermal equilibrium with their environment, in this case at 10 K, also referred to as “hot atom” chemistry). Consequently, the lower fluence of the cosmic-ray field is clearly eliminated by the capability of cosmic-ray MeV particles to generate multiple reactive atoms within a single collision cascade (Kaiser et al. 1997). Charged particles divert their kinetic energy via electronic and nuclear interaction to the ice target, and the ratio of this electronic versus nuclear energy transfer depends strongly on the kinetic energy of the implant. For example, solar wind particles have kinetic energies on the order of 1 keV amu⁻¹; they interact predominantly (>95%) through nuclear (elastic) interaction processes. On the other hand, 10 MeV cosmic-ray particles, as present in the deep interior of cold clouds, lose their energy almost exclusively (99.999%) via electronic interaction to the target molecules. As a high-energy cosmic-ray particle penetrates an ice, it produces an “infratrack” (or “primary ionization track”) a few angstroms perpendicular to the trajectory, within which these electronic interaction processes lead primarily to bond ruptures and ionization of the molecules. Detailed collision cascade calculations show that in molecular crystals, up to a few keV could be transferred from the implant into a single molecule. Considering the ionization energy of, for example, methane of 12.7 eV, this few keV of energy is sufficient to form not only singly, but also multiply positively charged CH₄ⁿ⁺ ions. During the ionization process, secondary electrons are released, named δ -electrons (or δ -rays), which leave the molecule almost perpendicularly to the trajectory of the cosmic-ray implant and have a range of a few hundreds of nanometers, generating an “ultratrack” around the infratrack, leading to further bond rupture processes via inelastic energy transfer from the δ -electrons to the molecules residing within the ultratrack. Within the infratrack, the departing electrons leave positive charges behind; this can lead to Coulomb explosions, either intramolecular (within one molecule) or intermolecular (repulsion of various charged CH₄ⁿ⁺ ions), and generates more suprathreshold atoms and ions with kinetic energies of up to a few keV. The chemical nature of these particles depends on the composition of the ices, but is dominated by H/H⁺ with minor contributions of atoms/ions of oxygen, carbon, and nitrogen. Henceforth, the electronic energy transfer process generates suprathreshold species inside the infratrack via a conversion of potential energy into kinetic energy. These considerations suggest that in order to untangle the cosmic radiation field-induced formation of acetaldehyde in interstellar ices and to extract the underlying mechanisms comprehensively, it is necessary to carry out three discrete batches of irradiation experiments: (1) UV photolysis to mimic the internal UV field; (2) a charged particle irradiation of ices by keV protons and ions of oxygen, carbon, and nitrogen to simulate the suprathreshold particles generated via Coulomb explosion; and (3) keV electron bombardment of ice samples to mimic the δ -electrons in the ultratrack. In this paper, we focus on keV electron bombardment and hence the formation of acetaldehyde via electronic energy transfer processes, which contributes to about 99% of the energy loss of the Galactic cosmic-ray particles; the charged particle and photon-induced syntheses of acetaldehyde are subjects of forthcoming articles.

In our experiments the ices are processed by bombardment with 5 keV electrons. The Galactic cosmic-ray field consists predominantly of protons, which have a distribution maximum of

about 10 MeV and lose 99.99% of their kinetic energy via transfer of their kinetic energy to the electronic system of the target molecules (here carbon monoxide and methane). This electronic energy transfer generates energetic electrons (δ -electrons) with energies of a few keV; in addition, the electronic linear energy transfer (LET) of MeV protons to the ice target holds a similar value as the 5 keV electrons used in the present experiments, i.e., a few keV μm^{-1} (Johnson 1990; Bennett et al. 2004). Therefore, our laboratory experiments mimic the formation of acetaldehyde in carbon monoxide–methane *neighboring* complexes via charged particles through electronic energy-loss processes in interstellar ices, as condensed on grains in molecular clouds at 10 K. Once the cold cloud passes through the hot molecular core stage, the elevated temperatures can cause the newly formed acetaldehyde molecules to sublime, whereby they are detected in the gas phase via radio telescopes.

2.2. Temperature Conditions

Since our primary goal is to untangle the formation of acetaldehyde in ices deep inside molecular clouds and the sublimation of the icy component in the hot molecular core stage, the irradiation experiments have to be carried out at 10 K. This temperature is representative for ices condensed on interstellar grain material (Tielens & Allamandola 1987). The hot core phase is simulated by simply warming up the target after the irradiation and monitoring the newly formed species on line and in situ (see § 3). Note that if ices sublime close to the embedded YSO, the subliming molecules may also be photolyzed (Stäuber et al. 2004). In the present simulation experiments, the destruction of the subliming molecules by photons is not considered, but it will be simulated in future experiments via photolysis of the ices during the warming up phase. Therefore, the extracted formation rates of acetaldehyde present upper limits (because of destruction processes in the gas phase) once the sublimation process is engaged in hot cores.

2.3. Chemical Composition

It is important to elucidate the possible mechanisms as to how acetaldehyde might be formed inside interstellar ices via electronic energy transfer processes. Synthetic routes are derived combining concepts of suprathreshold chemistry (Roessler 1992; Kaiser 2002) together with a classical retrosynthetic approach. This will ultimately identify those molecules that are potential precursors to the acetaldehyde molecule and guide the selection of ice mixtures in our simulation experiments. Figure 1 compiles the retrosynthetic approach comprehensively. Acetaldehyde holds three nonequivalent single bonds (σ bonds), which can be cleaved homolytically (both species retain one electron of the pair previously involved in the chemical bond) to yield the H + CH₂CHO (box 1), CH₃ + CHO (box 2), and CH₃CO + H (box 3) radical pairs (electronic states are omitted for clarity). Formally, the polyatomic radicals can undergo a second homolytic bond rupture to form H + H + HCCHO (box 1.1), H + H + H₂CCO (boxes 1.2, 3.1), H + CH₂ + HCO (boxes 1.3, 2.1), and H + CH₃ + CO (boxes 2.2, 3.2). The resulting atoms and radicals can recombine to yield four reactive systems that can essentially form acetaldehyde in interstellar ices: H₂ + HCCHO (R1), H₂ + H₂CCO (R2), CH₂ + H₂CO (R3), and CH₄ + CO (R4).

To actually design realistic simulation experiments, we have to compare these reactants with those molecules actually observed in interstellar ices. If one of the reactants has not been observed on icy grains, this system can be eliminated from being studied. Most importantly, the HCCHO molecule presents a

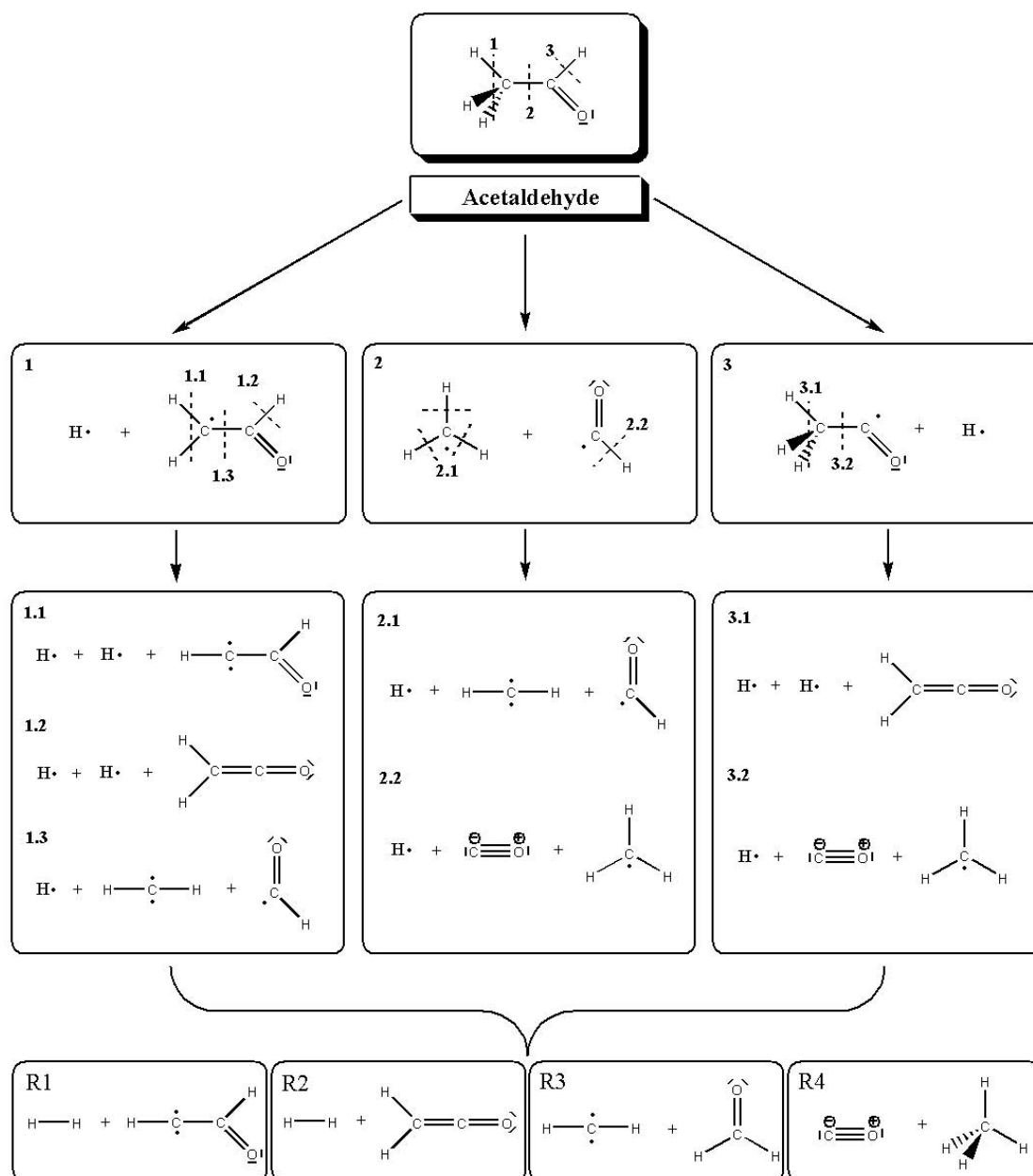


FIG. 1.—Retrosynthetic approach on the formation of acetaldehyde in extraterrestrial ices, which details that acetaldehyde can be formed by the recombination of the radical pairs in boxes 1, 2, and 3; these in turn can be formed by the recombination of the species shown in boxes 1.1–3, 2.1–2, and 3.1–2, which can be formed from a bond cleavage of the initial reactants R1–R4.

reactive carbene that has been detected neither in the gas phase nor in the solid state. Note that the carbene could undergo a [1,2]-hydrogen migration to yield the ketene molecule H_2CCO ; the latter presents also a necessary reactant in R2, but has only been observed in the gaseous interstellar medium. Likewise, the carbene diradical in R3 has not been detected in interstellar ices; therefore, R3 likely plays no role in the synthesis of acetaldehyde. Note, however, that suprathreshold carbene species can be generated inside methane-containing ices via nuclear interaction through inelastic energy transfer from a cosmic-ray particle to the CH_4 molecule (Kaiser & Roessler 1998). This possibility will be investigated in a forthcoming paper dealing exclusively with nuclear energy transfer processes.

With these considerations, R4 presents the only system whose reactants were observed in interstellar ices. Carbon monoxide has been identified in polar and apolar ice matrices toward quies-

cent dark clouds (Elias 16) and YSOs of low mass (Elias 29), intermediate mass (e.g., AFGL 989), and high mass (e.g., Orion BN, W33A, and AFGL 7009S); typically abundances from 3% to 30% (relative to water) are found (Tielens et al. 1991; Ehrenfreund et al. 1996; Schutte 1999; Gibb et al. 2000, 2004). Likewise, methane has also been identified in such regions, where abundances of 1%–6% are commonly found (Sandford et al. 1988; Boogert et al. 1996, 1997, 1998; Ehrenfreund et al. 1997; Gibb et al. 2000, 2004; Keane et al. 2001). It should, however, be noted that the majority (>70%) of the carbon monoxide detected is associated with an outer apolar layer, which is suspected to be composed mostly of CO, N_2 , and O_2 . Thus, we would not expect to find methane as a neighboring molecule to this fraction of the carbon monoxide detected; typically the polar abundance is closer to 2%–10% (Schutte 2002). However, *even if* carbon monoxide and methane may not be initially condensed

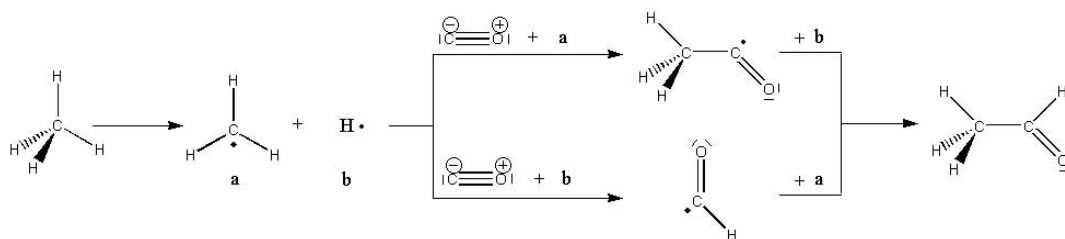


FIG. 2.—Proposed possible pathways to form acetaldehyde in carbon monoxide–methane ice mixtures via initial bond rupture of the methane molecule initiated by electronic energy transfer processes from the impinging energetic electron and two subsequent reaction channels to form the acetaldehyde molecule via reaction of either the radical (a) or atom (b) to the carbon monoxide molecule followed by barrierless recombination of the remaining radical or atom; electronic states are omitted for clarity.

onto a grain in proximity to one another, as they are both irradiation products from methanol we can still expect neighboring carbon monoxide and methane molecules to occur within interstellar ices (Baratta et al. 2002). Note that both carbon monoxide (2%–23%) and methane (1%) have also been assigned in cometary ices (Crovisier 1998; Biver et al. 2002). On the basis of these considerations, we selected CO/CH₄ mixtures to test whether acetaldehyde can be formed in interstellar ices via the reaction sequences outlined in Figure 2. Again, we would like to stress that no ices that contain solely carbon monoxide and methane have been identified so far. The choice of this ice mixture mimics rather neighboring CO–CH₄ molecules in astrophysical ices to address *specific mechanisms* of a high-energy induced formation of acetaldehyde in astrophysical ices.

3. EXPERIMENTAL APPROACH

The simulation experiments were carried out in a contamination-free ultrahigh vacuum (UHV) chamber; the top view of this machine is outlined in Figure 3. This setup consists of a 15 liter cylindrical stainless steel chamber of 250 mm diameter and 300 mm height, which can be evacuated down to 8×10^{-11} torr by a magnetically suspended turbopump backed by an oil-free scroll pump. A two-stage closed-cycle helium refrigerator, interfaced to a differentially pumped rotary feedthrough, is attached to the lid of the machine and holds a polished silver monocrystal. This crystal is cooled to 10.4 ± 0.3 K, serves as a substrate for the ice condensate, and conducts the heat generated from the impinging electrons to the cold head. To minimize the radiative heat transfer from the chamber walls to the target, a 40 K aluminum radiation shield is connected to the second stage of the cold head and surrounds the crystal. The ice condensation is assisted by a precision leak valve. The latter is connected to a gas reservoir and rests on a linear transfer mechanism; during the actual gas condensation, the deposition system can be moved to 5 mm in front of the silver target. This setup guarantees a reproducible thickness and composition of the frosts. To allow a selection of the target temperature, a temperature sensor, a 50 Ω cartridge heater, and a programmable controller are interfaced to the target.

The CO-CH₄ ices were prepared at 10 K by depositing premixed gases onto a cooled silver crystal. Blank checks of the pure gases (CH₄, 99.99%; CO, 99.99%; The Specialty Gas Group) via a quadrupole mass spectrometer (QMS) and of the frosts via a Fourier transform infrared (FTIR) spectrometer showed no acetaldehyde contamination in the samples. Table 1 compiles the absorptions present in the methane–carbon monoxide mixture. To determine the ice composition quantitatively, we integrated numerous absorption features and calculated the column density, i.e., the numbers of absorbing molecules per cm² inside the ice, via a modified Lambert-Beer relationship (Bennet et al. 2004). For carbon monoxide we used the ¹³CO isotope peak to quantify

the abundance (multiplied by 100/1.1 to get the total CO thickness), which was composed not only of the fundamental band appearing at 2090 cm⁻¹, but also a shoulder feature at 2086 cm⁻¹ (ratio of the areas $\sim 6:1$), which was attributed to the formation of a CO–CH₄ complex, similar to that observed in thin films of CO : CH₄ by Alsindi et al. (2003). For methane, we chose to use the weaker bands absorbing at 3849 cm⁻¹ ($3\nu_4$ overtone band) and 4203 cm⁻¹ ($\nu_1 + \nu_4$ combination band). The integrated absorption features, the corresponding integral absorption coefficients, and the column densities are summarized in Table 2. These data suggest a carbon monoxide–rich ice and a CO : CH₄ ratio of 6:1, with column densities of 2.9×10^{18} and 5.2×10^{17} cm⁻², respectively. Considering a density of 0.53 g cm⁻³ for CH₄ ice (Wyckoff 1965) and 1.03 g cm⁻³ for CO ice (Krupskii et al. 1973) at 10 K, this translates into a thickness of 0.26 ± 0.02 μm methane and 1.31 ± 0.05 μm carbon monoxide ices (giving an estimated total ice thickness of 1.57 ± 0.05 μm).

These ices were irradiated isothermally at 10 K with 5 keV electrons generated in an electron gun (Specs EQ-22/35) at beam currents of 100 nA (30 minutes) by scanning the electron beam over an area of 3.0 ± 0.4 cm². Accounting for irradiation times, as indicated in parentheses, and the extraction efficiency of 78.8% of the generated electrons, this exposes the target to 8.8×10^{14} electrons. Higher beam currents should be avoided to rule out overlapping cascades and to limit the temperature increase of the frost surface to less than 1 K. After the actual irradiation, the sample was kept isothermal at 10 K for 60 minutes and heated then by 0.5 K minute⁻¹ to 273 K. We used the CASINO code (Drouin et al. 2001) to simulate the electron trajectories within the ice, with input parameters defined by our previously determined CO : CH₄ ratio. The results give a distribution maximum at a penetration depth of 620 nm, therefore exposing our sample to an *average* dose of 1.1 ± 0.2 eV per molecule and giving us an average LET of 8 keV μm^{-1} .

To guarantee an identification of the reaction products in the ices and those subliming into the gas phase on line and in situ, two detection schemes are incorporated: (1) an FTIR spectrometer and (2) a QMS. The chemical modifications of the ice targets are monitored during the experiments to extract time-dependent concentration profiles and hence production rates of newly formed molecules and radicals in the solid state. The latter is sampled via a Nicolet 510 DX FTIR spectrometer (6000–500 cm⁻¹) operating in an absorption-reflection-absorption mode (reflection angle $\alpha = 75^\circ$; Fig. 3), each spectrum comprising 282 scans operating at a resolution of 2 cm⁻¹. The infrared beam is coupled via a mirror flipper outside the spectrometer, passes through a differentially pumped potassium bromide (KBr) window, is attenuated in the ice sample prior to and after reflection at a polished silver wafer, and exits the main chamber through a second differentially pumped KBr window before being monitored

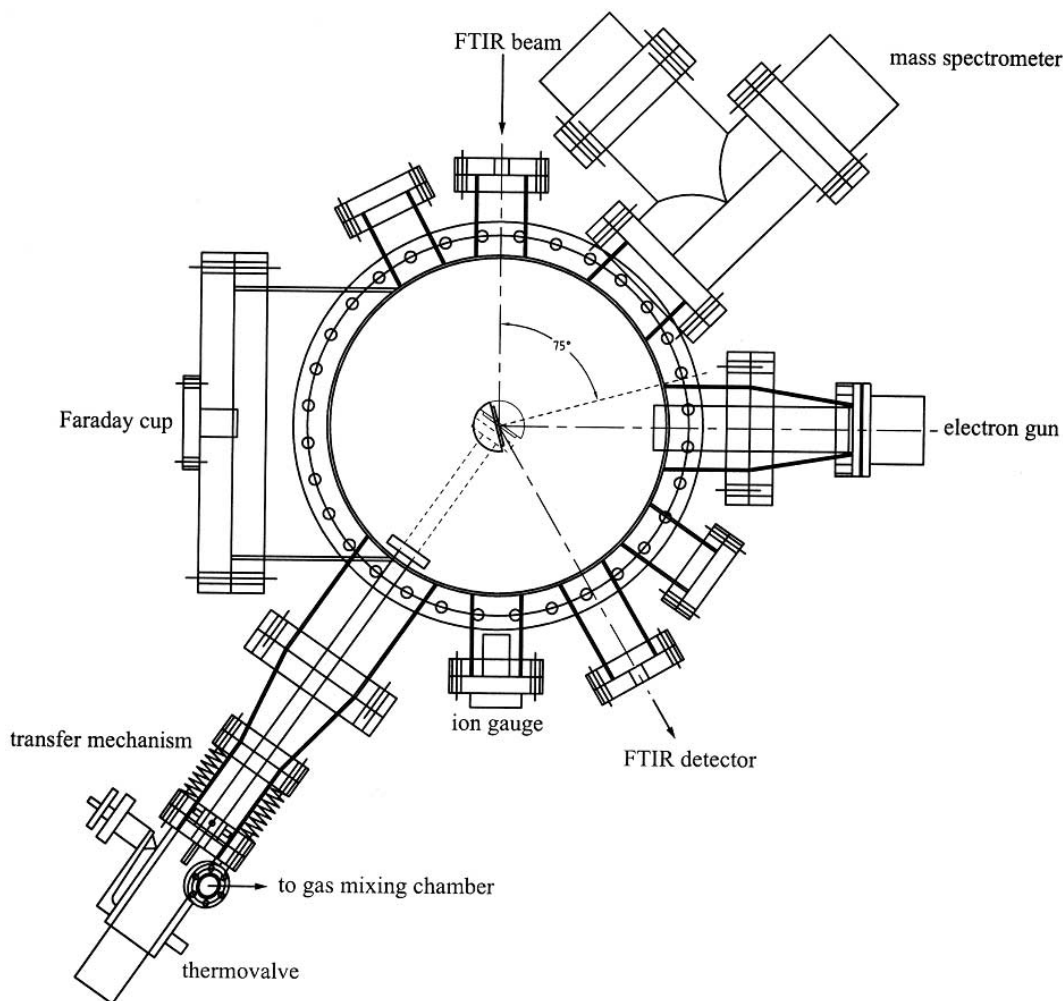


FIG. 3.—Top view of the experimental setup. The cooled silver mirror target (10 K) is rotated to face a glass capillary array attached to the linear transfer mechanism, which is extended to within 5 mm of the target, and the CO : CH₄ mixture is deposited via a precision leak valve. Then the target is rotated and aligned with the FTIR to a reflection angle of 75°, where it remains throughout the irradiation from the electron gun and during the warm-up process so that newly formed species can be detected. Species subliming into the gas phase are monitored throughout via the mass spectrometer.

TABLE 1
INFRARED ABSORPTIONS OF THE CARBON MONOXIDE–METHANE FROST AT 10 K (6:1)

Band Position [cm ⁻¹ (μm)]	Assignment	Characterization
2906 (3.44).....	ν_1 (CH ₄)	Symmetric stretch
1529 (6.54).....	ν_2 (CH ₄)	Degenerate deformation
3003 (3.33), 3018 (3.31).....	ν_3 (CH ₄)	Degenerate stretch
1295 (7.72), 1308 (7.65).....	ν_4 (CH ₄)	Degenerate deformation
2595 (3.85).....	$2\nu_4$ (CH ₄)	Overtone
3849 (2.60).....	$3\nu_4$ (CH ₄)	Overtone
2817 (3.55).....	$\nu_2 + \nu_4$ (CH ₄)	Combination
4118 (2.43).....	$\nu_2 + 2\nu_4$ (CH ₄)	Combination
4203 (2.38).....	$\nu_1 + \nu_4$ (CH ₄)	Combination
4301 (2.33).....	$\nu_3 + \nu_4$ (CH ₄)	Combination
4529 (2.21).....	$\nu_2 + \nu_3$ (CH ₄)	Combination
2142 (4.67).....	ν_1 (CO) (apolar)	C–O stretch
2090 (4.79), 2086sh (4.79).....	ν_1 (¹³ CO)	Isotope peak, [¹³ CO–CH ₄] complex
4247 (2.36).....	$2 \nu_1$ (CO)	Overtone

NOTE.—Assignment of the observed bands according to Kaiser et al. (1998) (CH₄), Sandford et al. (1988), Zou & Varanasi (2002), and Alsindi et al. (2003) (CO).

TABLE 2
INTEGRAL ABSORPTION COEFFICIENTS USED TO DETERMINE THE COLUMN DENSITIES OF METHANE
AND CARBON MONOXIDE, INTEGRATED PEAK AREA OF THE ABSORPTIONS IN OUR EXPERIMENTS,
AND ESTIMATED TARGET THICKNESS OF THE CARBON MONOXIDE AND METHANE ICES

Peak Limits (cm ⁻¹)	Peak Area (cm ⁻¹)	<i>A</i> (cm molecule ⁻¹)	<i>n</i> (molecules cm ⁻²)	<i>d</i> (μm)
4226–4180	2.909	1.6 × 10 ⁻¹⁸	5.42 × 10 ¹⁷	0.27
3859–3841	0.328	2.0 × 10 ⁻¹⁹	4.89 × 10 ¹⁷	0.25
2096–2072	1.395	1.3 × 10 ⁻¹⁷	2.91 × 10 ¹⁸	1.31

NOTES.—Integral absorption coefficients were taken from Kaiser et al. (1998) (methane) and Gerakines et al. (1995) (carbon monoxide). Note that the ¹³CO peak is multiplied by 100/1.1 to get the total CO thickness.

via a liquid nitrogen-cooled detector (mercury-cadmium-telluride detector type B [MCTB]). Compared to room temperature DTGS (deuterated triglycine sulfate) detectors and a data accumulation in transmission mode, two effects enhance the sensitivity of this detection scheme by almost 2 orders of magnitude. These are (1) the lower background noise level of our liquid nitrogen-cooled detector by a factor of 10 compared to room temperature detectors and (2) the operation of the spectrometer in absorption-reflection-absorption mode rather than in transmission mode, which enhances the sensitivity by a factor of $f = 2/\cos \alpha \approx 8$; the factor 2 accounts for the fact that the beam passes the sample twice (incoming and outgoing beam). The gas phase is monitored by a quadrupole mass spectrometer (Balzer QMG 420; 1–200 amu mass range) with electron impact ionization of the neutral molecules in the residual gas analyzer mode at electron energies of 90 eV.

4. ELECTRONIC STRUCTURE CALCULATIONS

We have examined the C₂H₄O potential energy surface of the reaction of methane (CH₄) with carbon monoxide (CO) in the gas phase in terms of ab initio molecular orbital methods. In this paper, we focus on the initial carbon-hydrogen bond cleavage of the methane molecule and the successive reaction of the fragments, i.e., the potential energy surfaces of H(²S_{1/2}) + CO(*X*¹Σ⁺) and CH₃(*X*²A₂') + CO(*X*¹Σ⁺). Although the reaction pathways of H(²S_{1/2}) + CO(*X*¹Σ⁺) → HCO(*X*²A') and CH₃(*X*²A₂') + CO(*X*¹Σ⁺) → CH₃CO(*X*²A') have been studied extensively in previous papers (see our discussion), we also explored the formation pathways of the corresponding HOC and CH₃OC isomers. We employed the hybrid density functional B3LYP method (Lee et al. 1988; Becke 1993) with the 6-311G(d,p) basis functions in order to optimize the molecular structures at the energy minima and transition states. The relative energies were refined by using the coupled cluster CCSD(T) method (Purvis & Bartlett 1982; Raghavachari et al. 1989) with the aug-cc-pVTZ basis functions (Dunning 1989) at the structures obtained by the B3LYP method. All relative energies were corrected by the zero-point vibrational energies calculated with the B3LYP method without scaling. We use the CCSD(T) values for the discussion of energetics in this paper, as they correlate more accurately to the experimental results. All calculations were carried out with the Gaussian 98 program package (Frisch et al. 2001). In order to analyze the infrared spectra for the species obtained by the present experiments, we have calculated the vibrational frequencies and infrared intensities for the structures obtained with the B3LYP/6-311G(d,p) method (Table A1, below). Comparison of the experimental data with the theoretical calculations of the vibrational frequencies suggests that a scaling factor of 0.98 should be applied. The infrared intensities

are accurate within 20% at this level of theory (Galabov et al. 2002).

5. RESULTS

5.1. Computational Results

Figure 4 shows the potential energy surfaces and optimized geometries at the stationary points (all energies given are relative to the initial reactants) of H(²S_{1/2}) + CO(*X*¹Σ⁺) → HCO(*X*²A')/HOC(*X*²A') in the top left of the figure, CH₃(*X*²A₂') + CO(*X*¹Σ⁺) → CH₃CO(*X*²A')/CH₃OC(*X*²A') in the top right, and finally the complete CH₃CHO(*X*¹A') → CH₄(*X*¹A₁) + CO(*X*¹Σ⁺) at the bottom. Note that the relative energies are not altered whether the reaction proceeds forward or backward. In order to demonstrate how these potential energy surfaces can give us detailed insights into the expected formation routes in our experiment, recall that our proposed synthesis of acetaldehyde (see Fig. 2) is based initially on the cleavage of a carbon-hydrogen bond in the methane molecule. Since energy barriers tend to be underestimated with the B3LYP method, the relative energies that should be used for the discussion of energetics in this system are the values obtained with the CCSD(T) method, which are shown in parentheses in Figure 4 and also listed in Table 3. The electronic structure calculations indicate that the initial carbon-hydrogen bond cleavage of the methane molecule is endoergic by 427 kJ mol⁻¹ (bear in mind that CH₄ + CO lies 27 kJ mol⁻¹ below acetaldehyde in the diagram), which is in good agreement with an experimental value of 454 kJ mol⁻¹. We must now turn to the fate of the radicals produced and how they may subsequently react with carbon monoxide, specifically the reactions of H(²S_{1/2}) + CO(*X*¹Σ⁺) and CH₃(*X*²A₂') + CO(*X*¹Σ⁺) to form HCO(*X*²A'), HOC(*X*²A'), CH₃CO(*X*²A'), and CH₃OC(*X*²A'). All four reactions have entrance barriers of the hydrogen atom or methyl radical attack to carbon monoxide. The calculated energies with the B3LYP and CCSD(T) methods and the enthalpies obtained with the G2 (Curtiss et al. 1991) and G3 (Curtiss et al. 1998) methods are compared with the experimental heats of formation in Table 3. All theoretical values are in good agreement with the experimental data, although the experimental values cited from Smith et al. (1991) differ slightly from those data obtained from the NIST Web site.⁵

We have calculated an energy barrier of 11.2 kJ mol⁻¹ and a heat of formation of -59.5 kJ mol⁻¹ for the reaction H(²S_{1/2}) + CO(*X*¹Σ⁺) → HCO(*X*²A'); the barrier for the reverse reaction [hydrogen elimination from HCO(*X*²A')] is therefore calculated to be 70.7 kJ mol⁻¹. Keller et al. (1996), Woon (1996), and Jursic (1998) studied this system extensively and reported that the best estimated theoretical values of the energy barrier and the heat

⁵ See <http://webbook.nist.gov/chemistry>.

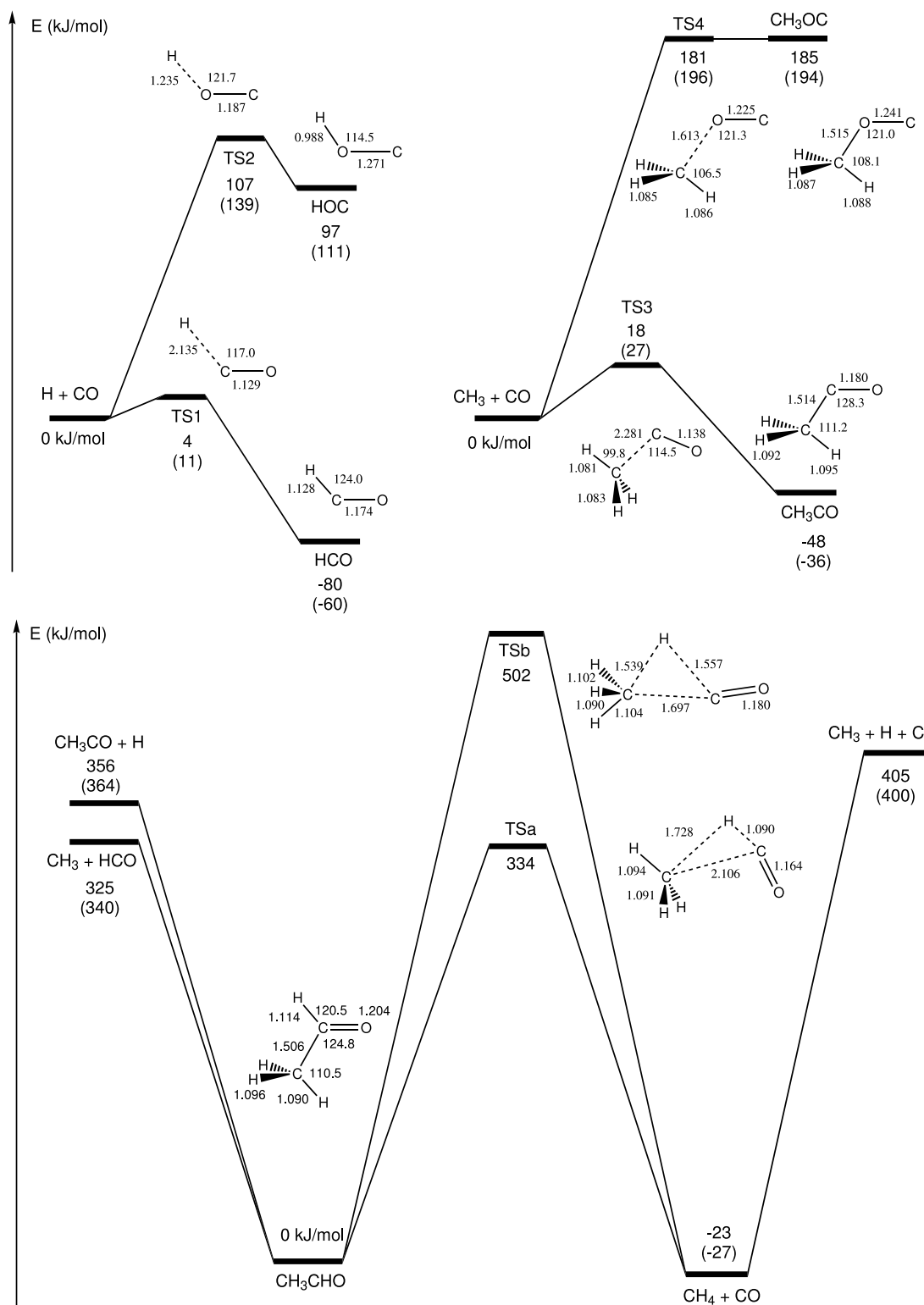


FIG. 4.—Schematic potential energy surfaces of the methane–carbon monoxide system: hydrogen reacting with carbon monoxide (top left), methyl radical with carbon monoxide (top right), and the formation/dissociation pathways of acetaldehyde and carbon monoxide/methane (bottom).

of the reaction are 10.5 and $-59.8 \text{ kJ mol}^{-1}$, respectively. The corresponding experimental values are 8.3 ± 1.7 (Wang et al. 1973) and $-58.6 \text{ kJ mol}^{-1}$ (Werner et al. 1995), respectively. The heat of formation calculated from the values of the NIST Web site gives -64 kJ mol^{-1} for the same reaction, which is slightly larger than the values mentioned above. The formation of the $\text{HOC}(X^2A')$ radical is calculated to be 111 kJ mol^{-1}

endoergic and has a barrier (TS2) of 139 kJ mol^{-1} , while the energy barrier of hydrogen elimination (TS2) from $\text{HOC}(X^2A')$ is calculated to be 28 kJ mol^{-1} .

For the reaction $\text{CH}_3(X^2A_2'') + \text{CO}(X^1\Sigma^+) \rightarrow \text{CH}_3\text{CO}(X^2A')$, we calculate an energy barrier of 38 kJ mol^{-1} and a heat of formation of -36 kJ mol^{-1} . The reverse of this process is the dissociation of the $\text{CH}_3\text{CO}(X^2A')$ species, as observed as one of

TABLE 3
 EXPERIMENTAL AND THEORETICAL VALUES OF REACTION ENTHALPIES IN kJ mol⁻¹

Reaction	Experimental ^a	Experimental (ΔH) ^b	B3LYP	CCSD(T) (ΔE)	G2 (ΔH)	G3 (ΔH)
H + CO → HCO.....	-58	-64	-80	-60	-61	-63
H + CO → HOC.....	97	111	117	114
CH ₃ + CO → CH ₃ CO.....	-51	-47	-48	-36	-41	-39
CH ₃ + CO → CH ₃ OC.....	185	194	194	197
CH ₃ + HCO → CH ₃ CHO.....	-348	-360	-325	-340	-357	-347
CH ₃ CO + H → CH ₃ CHO.....	-355	-377	-356	-364	-378	-372
CH ₃ + H + CO → CH ₃ CHO.....	-406	-439	-405	-400	-418	-410
CH ₃ CHO → CH ₄ + CO.....	-26	-15	-23	-27	-25	-23

^a Reference from Smith et al. (1991). Note that at $T = 0$ K, reaction energies and enthalpies are identical.

^b Taken from the NIST database, <http://webbook.nist.gov/chemistry>.

the secondary decomposition products in the photodissociation of acetyl derivatives (North et al. 1994; Kurosaki & Yokoyama 2003). Our computed value of the barrier involved in the decomposition of CH₃CO(*X*²*A'*) of 74 kJ mol⁻¹ agrees very well with a recent experimental value of 71 kJ mol⁻¹ (North et al. 1994). The potential energy surface for this reaction has also been extensively studied (Yadav & Goddard 1986; Belbruno 1997; Mordaunt et al. 1998); in comparison of our calculated value of -36 kJ mol⁻¹ for the heat of formation with a recent theoretical CASSCF calculation by Diau et al. (2002), a value of -58 kJ mol⁻¹ is given. This value, however, seems to be overestimated, and the heat of formation from the NIST database gives -47.2 kJ mol⁻¹. Although our CCSD(T) value of -36 kJ mol⁻¹ might be too small compared to the experimental heat of formation, the G2 and G3 methods also give similar values of -41 and -39 kJ mol⁻¹, respectively. Note that the barrier of the methyl radical addition is larger by about 27 kJ mol⁻¹ compared to the addition of the hydrogen atom to carbon monoxide. The formation of the CH₃OC(*X*²*A'*) species from the methyl radical and carbon monoxide is much more endoergic (+194 kJ mol⁻¹) than the formation of HOC(*X*²*A'*), and the transition state TS4 of the C-O bond cleavage of the CH₃OC(*X*²*A'*) radical is calculated to be only 2 kJ mol⁻¹—the energy of TS4 obtained with B3LYP method becomes lower than that of CH₃OC(*X*²*A'*) when we correct the zero-point vibrational frequencies.

This may indicate that the CH₃OC(*X*²*A'*) radical may not lie in an energy minimum and, if formed, would instantaneously dissociate back to the reactants, therefore being unlikely to be observable in our experiment, whereas the HOC(*X*²*A'*) radical is located at the energy minimum and should be experimentally observable. We have also tried to find the transition state of the isomerization from HOC(*X*²*A'*) and CH₃OC(*X*²*A'*) to HCO(*X*²*A'*) and CH₃CO(*X*²*A'*), but we were unsuccessful.

Note that with regard to the formation of acetaldehyde, both of the reactions CH₃(*X*²*A'*) + HCO(*X*²*A'*) → CH₃CHO(*X*¹*A'*) and CH₃CO(*X*²*A'*) + H(²*S*_{1/2}) → CH₃CHO(*X*¹*A'*) were found to proceed without barrier and to be exoergic by 340 and 364 kJ mol⁻¹, respectively; since both reactants are open-shell species, this is not surprising. Finally, we should stress that we also found two transition states for the one-step reaction of methane with carbon monoxide to acetaldehyde; however, the transition states isolated (TSa and TSb) are very high in energy compared to the separated reactants.

5.2. Infrared Spectroscopy

The analysis of the infrared spectra is carried out in three consecutive steps. First, we investigate the new absorptions quali-

tatively and assign their carriers. Then, the temporal developments of these absorptions upon electron irradiation are investigated quantitatively as outlined in § 3. Finally, these data are fitted to calculate production rates of synthesized molecules in units of molecules cm⁻² (column density).

5.2.1. Qualitative Analysis

As the focus of this paper is on the formation of acetaldehyde, the focus of this section is on the identification of only species relevant to acetaldehyde formation. The effects of the electron bombardment of the binary ice mixtures are compiled in Figures 5a–5f. We also compare our experimental results with recent experiments carried out by Moore & Hudson (2003), whereby binary ice mixtures of CO : CH₄ at ratios of 50 : 1 and 100 : 1 were irradiated with UV irradiation from a microwave-discharged hydrogen flow lamp and 0.8 MeV protons, respectively. A comparison of the unirradiated sample with the exposed ices at 10 K clearly identifies novel absorption features of the methyl radical [CH₃(*X*²*A'*)] at 612 cm⁻¹ (ν_2 [out of plane]; Fig. 5a; Tables 4 and A1). The position of this band is in close concurrence with previous matrix isolation studies of the methyl radical in neon (617 cm⁻¹; Snelson 1970), argon (603 cm⁻¹; Milligan & Jacox 1967), and nitrogen (611 cm⁻¹; Milligan & Jacox 1967) samples. Moore & Hudson (2003) were able to identify the same feature for the methyl radical located at 619 cm⁻¹.

We were also able to identify the formyl radical [HCO(*X*²*A'*)] in all irradiated samples at 1853 cm⁻¹ (ν_3 [CO stretch]) and 1090 cm⁻¹ (ν_2 [bending mode]; Figs. 5b and 5c; Tables 4 and A1). Both peak positions are also in nice agreement with previous matrix studies depicting bands at 1863 cm⁻¹ (argon; Milligan & Jacox 1969), 1858 cm⁻¹ (xenon; Pettersson et al. 1999), and 1861 cm⁻¹ (carbon monoxide; Ewing et al. 1960; Milligan & Jacox 1964), as well as 1087 cm⁻¹ (argon; Milligan & Jacox 1969) and 1090 cm⁻¹ (carbon monoxide; Ewing et al. 1960; Milligan & Jacox 1964). Moore & Hudson (2003) were able to assign bands at 2489, 1859, and 1090 cm⁻¹ to the formyl radical [HCO(*X*²*A'*)]; however, the reaction mechanisms to form these species were not discussed by these authors.

Finally, four absorptions at 1728, 1351, 1123, and 1426 cm⁻¹ could be attributed to the ν_4 (CO stretching), ν_7 (CH₃ deformation), ν_8 (CH₃ deformation), and ν_{12} (CH₃ deformation) modes of the acetaldehyde molecule [CH₃CHO(*X*¹*A'*)], respectively (Figs. 5c–5f; Tables 4 and A1). Note that the ν_4 band is quite sensitive to its environment; it is shifted to a lower wavenumber with respect to the gas phase at 1743 cm⁻¹, but to a higher wavenumber compared to the liquid phase at 1714 cm⁻¹ (Shimanouchi 1972). Moore & Hudson (2003) were also able to identify acetaldehyde

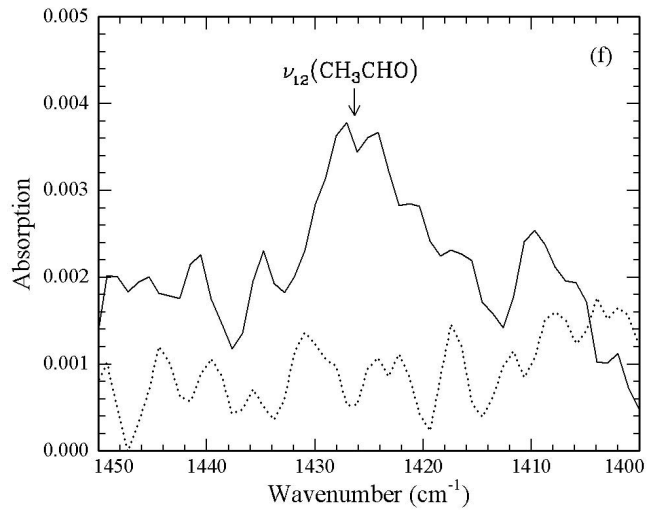
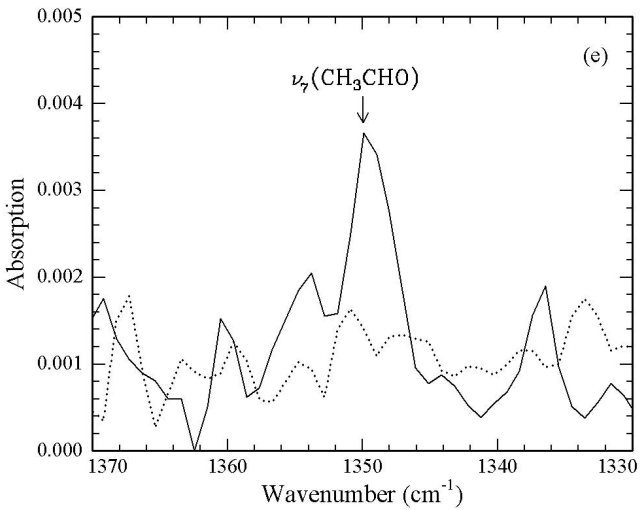
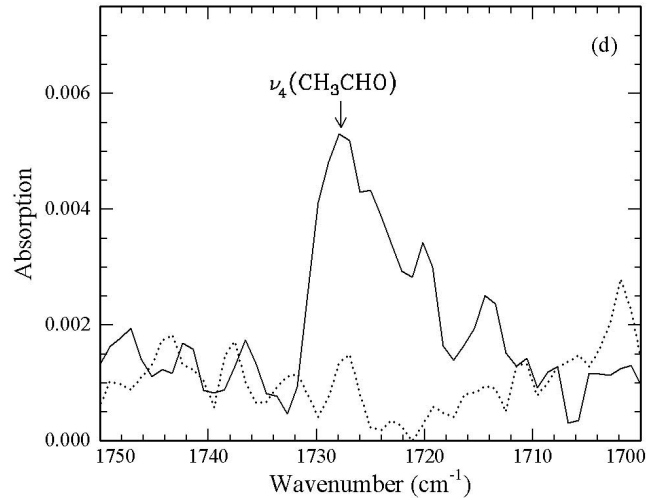
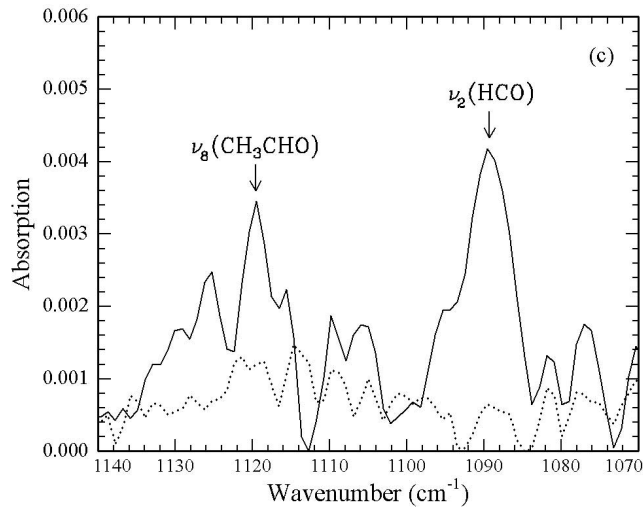
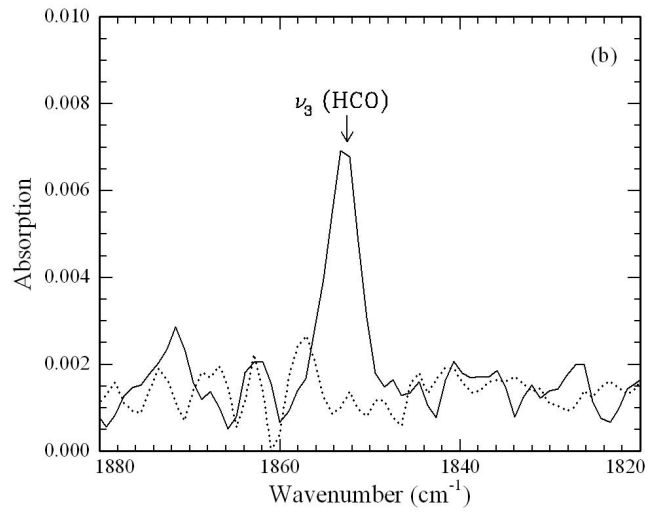
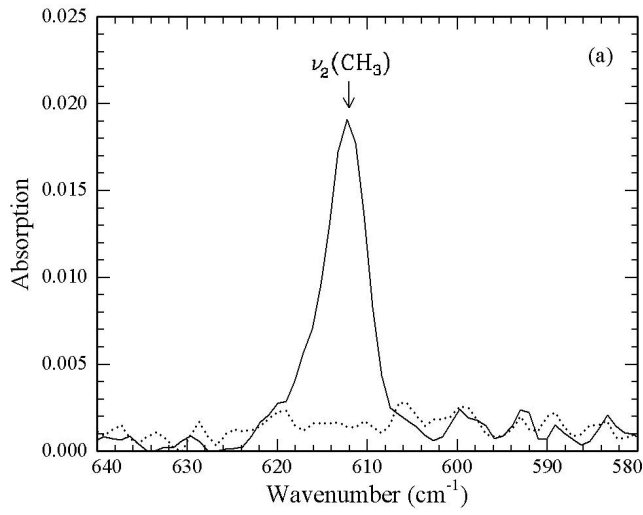


Fig. 5.—(a–f) New absorption features in the CO/CH₄ ice mixture before (*dashed line*) and after (*solid line*) 30 minutes of irradiation of 5 keV electrons at 100 nA. For further information please refer to the text and Table 4.

TABLE 4
NEW INFRARED ABSORPTIONS OF THE PROCESSED CARBON MONOXIDE–METHANE SAMPLE
AND CALCULATED INTEGRAL ABSORPTION COEFFICIENTS

Observed Frequency [cm ⁻¹ (μm)]	Species	Assignment	<i>A</i> (cm molecule ⁻¹)
612 (6.43).....	CH ₃	ν ₂ (out of plane)	1.4 × 10 ⁻¹⁷
1853 (5.40).....	HCO	ν ₃ (CO stretch)	1.5 × 10 ⁻¹⁷
1090 (9.17).....	HCO	ν ₂ (bending)	5.5 × 10 ⁻¹⁸
1728 (5.79).....	CH ₃ CHO	ν ₄ (CO stretch)	3.0 × 10 ⁻¹⁷
1351 (7.40).....	CH ₃ CHO	ν ₇ (CH ₃ deformation)	4.5 × 10 ⁻¹⁸
1123 (8.91).....	CH ₃ CHO	ν ₈ (CH ₃ deformation)	4.3 × 10 ⁻¹⁸
1426 (7.01).....	CH ₃ CHO	ν ₁₂ (CH ₃ deformation)	3.6 × 10 ⁻¹⁸

NOTE.—All values for a sample at 10 K and after an irradiation time of 30 minutes (see text for details).

at 1727, 1429, 1349, and 1122 cm⁻¹. Hawkins & Andrews (1983) also observed acetaldehyde when they irradiated mixtures of Ar : O₃ : C₂H₄ (200 : 2 : 1) by UV irradiation from a mercury arc lamp. They observed acetaldehyde at 1731, 1430–1435, 1350–1354, 1121, and 774 cm⁻¹. Recently, Schriver et al. (2004) irradiated thin films of ethylene oxide (c-C₂H₄O) in rare gas matrices, as a pure ice, and in water mixtures with UV irradiation from a microwave-discharged hydrogen flow lamp. They found that in irradiated ices of pure ethylene oxide, they observed bands at 1719, 1429, 1349, 1122, and 770 cm⁻¹, which were attributed to acetaldehyde. In our experiments we also observed a peak at 759 cm⁻¹; however, comparison of the theoretical intensities (Table A1) with the ratios of the peak areas lead us to conclude that the absorption was too strong to be associated solely to acetaldehyde, although it could be a minor contributor. Experiments carried out by Jacox (1982) on the irradiation of acetaldehyde showed that the absorbance at 765 cm⁻¹ in their experiments could be attributable to the formyl methyl radical [CH₂CHO(*X*²*A'*)]. Note that we were unable to identify any absorptions of the acetyl radical [CH₃CO(*X*²*A'*)] around 1840 cm⁻¹ and in the 1330–1420 cm⁻¹ region (Jacox 1982). We were also unable to detect any absorptions that could be associated with either of the more unstable isomers, HOC(*X*²*A'*) and CH₃OC(*X*²*A'*).

5.2.2. Quantitative Analysis

Figures 6a and 6b depict the temporal development of the column density of the carbon monoxide and methane reactant

molecules based on the absorption bands, as discussed in § 3. Figures 7a–7c show the temporal development of the methyl radical, formyl radical, and acetaldehyde products. The choice of baseline represents the largest source of error upon peak integration; the error bars shown in the figures are given as 1 σ values. The integrated absorption coefficients used to quantify the column densities of the reactants are the same as those discussed in § 3 (Table 2). The integrated absorption coefficients used to calculate the column densities of the products are listed in Tables A1 and 4; note that we use theoretical values for the intensities. Although, again, there has been some work carried out attempting to put experimental values to the intensities of radicals, the values derived previously will always have a large uncertainty attributed to the fact the measurements are always taken indirectly, as the radicals must be made in situ. In the case of the formyl radical, for example, we can refer to examples from Gerakines et al. (1996), wherein an *assumed* value for the ν₃ fundamental integrated absorption coefficient was listed as 1.0 × 10⁻¹⁷ cm molecule⁻¹; an experimental upper limit of 2.1 × 10⁻¹⁷ cm molecule⁻¹ has been given as an upper limit from Hudson & Moore (1999). Therefore, our theoretical value of 1.48 × 10⁻¹⁷ cm molecule⁻¹ is quite reasonable. Acetaldehyde also has a lack of data regarding its solid-state band strengths; values given for the ν₄ and ν₇ fundamentals listed as 1.3 × 10⁻¹⁷ and 1.5 × 10⁻¹⁸ cm molecule⁻¹, respectively, by Schutte et al. (1999) are traced back to Wexler (1967), from a study that covered aldehydes in general, but did not specifically mention acetaldehyde. Being

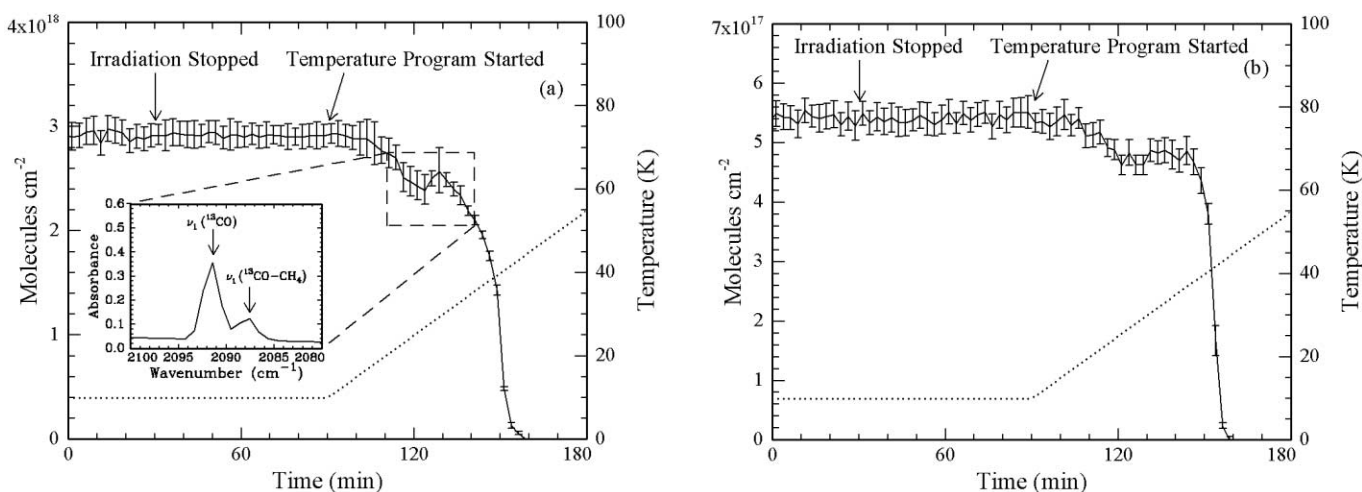


FIG. 6.—Temporal development of the column density of the reactant molecules: (a) carbon monoxide calculated via the integrated absorption for ν₁ (¹³CO) at 2090 cm⁻¹ and (b) methane calculated via the integrated absorption for ν₁ + ν₄ (CH₄) at 4203 cm⁻¹ during the experiment, the isothermal phase, and the heating period. The corresponding temperature profile is overlaid (dotted line).

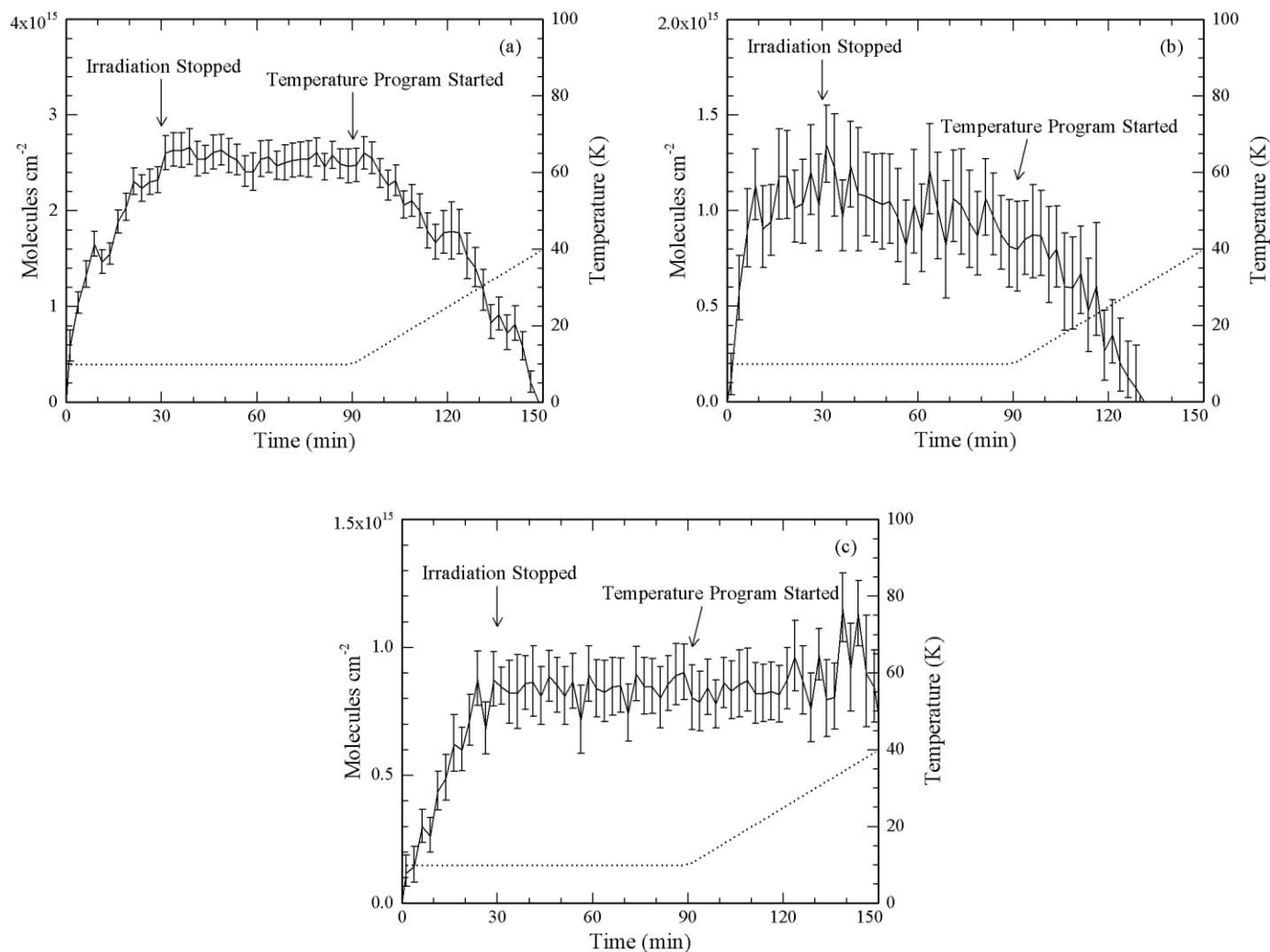


FIG. 7.—Temporal development of the column density of (a) the methyl radical calculated via the integrated absorption at 612 cm^{-1} , (b) the formyl radical calculated via the integrated absorption at 1090 cm^{-1} , and (c) the acetaldehyde molecule calculated via the integrated absorption at 1728 cm^{-1} during the experiment, the isothermal phase, and the heating period. The corresponding temperature profile is overlaid (dotted line).

a stable molecule rather than a radical, some solid-state information has been measured for a $\text{H}_2\text{O}:\text{CH}_3\text{CHO}$ (20:1) mixture,⁶ from which a value of $6.1 \times 10^{-18}\text{ cm molecule}^{-1}$ was derived for the ν_7 fundamental (Moore & Hudson 1998). Thus, our theoretical values of 2.97×10^{-17} (ν_4) and 4.5×10^{-18} (ν_7) cm molecule^{-1} again compare favorably to and are more reliable than previous studies. The column densities of the methyl radical, formyl radical, and acetaldehyde after irradiation of the products are $(2.23 \pm 0.38) \times 10^{15}$, $(9.04 \pm 1.47) \times 10^{14}$, and $(8.73 \pm 4.54) \times 10^{14}$, which, if we account for the area and electron current, gives us 7.6 ± 1.5 , 3.1 ± 0.6 , and 3.0 ± 1.8 species of the methyl radical, formyl radical, and acetaldehyde, respectively, produced per implanted electron.

Within the error limits, the column densities of the reactants, carbon monoxide and methane, as well as the products, the methyl radical, formyl radical, and acetaldehyde, all remain constant during the isothermal stage (with the formyl radical possibly being the only exception, which does appear to decrease slightly during this time frame). Upon the initiation of the heating program, however, we note an immediate decrease in the column densities for both the methyl radical and the formyl radical, characteristic of their enhanced mobility and subsequent reaction

(destruction). Carbon monoxide sublimates at around 30 K, whereas methane typically sublimates around 35–50 K (Alsindi et al. 2003). For the carbon monoxide, the column density becomes slightly erratic between 20 and 30 K, where the shoulder feature at 2086 cm^{-1} appears to increase slightly; this could be due to the fact that the binding energy of carbon monoxide within the $\text{CO}-\text{CH}_4$ complex ($\sim 14\text{ kJ mol}^{-1}$) is higher than in pure carbon monoxide ($\sim 7.6\text{ kJ mol}^{-1}$). The presence of the reactant/product falls can no longer be observed spectroscopically at 30 K (formyl radical), 39 K (methyl radical), and 44 K (methane and carbon monoxide), whereas acetaldehyde actually remains observable until 180 K (not shown in Fig. 7c).

5.3. Mass Spectrometry

In comparison of the infrared observations with the mass spectrometric analysis of the gas phase, during the irradiation phase of the sample only signal at $m/e = 2$ (H_2) was observed. The temporal development of the molecular hydrogen ion is shown in Figure 8. Since no CH_x species except methane and the methyl radical has been observed in the solid state, it is likely that the molecular hydrogen is formed via recombination of two hydrogen atoms in the matrix. In addition, we would like to emphasize that $m/e = 2$ presents the only signal detected with the mass spectrometer during the irradiation of the sample at 10 K

⁶ See <http://www-691.gsfc.nasa.gov/cosmic.ice.lab/spectra.htm>.

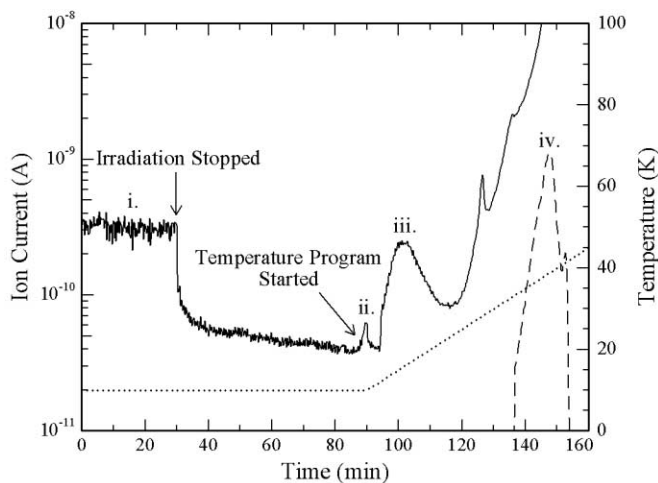


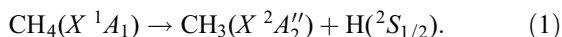
FIG. 8.—Temporal developments of the ion current of $m/e = 2$ (molecular hydrogen, *solid line*) and of $m/e = 43$ (the $C_2H_3O^+$ fragment ion of acetaldehyde, *dashed line*). The corresponding temperature profile is overlaid (*dotted line*). See § 5.3 for further details.

(Fig. 8 [i]). None of the CH_x ($x = 1-4$) species were found in the gas phase during the irradiation phase. This clearly demonstrates that $m/e = 2$ is not a fragment from methane molecules in the gas phase. The mass spectrometric data also show that after the irradiation, the matrix stores thermalized hydrogen atoms; these atoms diffuse upon warming of the matrix and recombine to form molecular hydrogen. The latter is released into the gas phase, starting at temperatures of 10–11 K, which may be from molecular hydrogen already formed but weakly bound to the surface (Fig. 8 [ii]). A larger amount of hydrogen is observed coming off between 12 and 21 K, which is likely to be from the recombination of the stored thermalized hydrogen atoms within the lattice and subsequent sublimation (Fig. 8 [iii]), although as all the methyl, formyl, and methane column densities are decreasing during this period, a thermal reaction involving the release of hydrogen cannot be ruled out. This result alone demonstrates the necessity of a sample temperature low enough, as done in the present experiments, to suppress the diffusion of thermalized hydrogen atoms (10 K); if the target temperature is too high, it is not feasible to discriminate between suprathreshold and thermal reaction mechanisms.

We also probed the temporal evolution of the acetaldehyde molecule. Since acetaldehyde has a mass-to-charge ratio m/e of 44, this pattern would overlap with carbon dioxide, which is also a product formed during the irradiation of carbon monoxide matrices (Gerakines et al. 1996; Jamieson et al. 2005). Therefore, we probed the acetaldehyde molecule at $m/e = 43$, i.e., at the $C_2H_3O^+$ fragment ion; note that this ion is unlikely to originate from any neutral C_2H_3O molecule, since neither CH_3CO nor CH_3OC was observed spectroscopically in our experiment. Again, no signal was detected during the irradiation and the isothermal phase. As the temperature increased to 34 K, the signal at $m/e = 43$ began to appear and increased; a maximum ion current was observed at 39 K (Fig. 8 [iv]). Note that it is now coming off with the bulk of the rest of the ice lattice.

6. DISCUSSION

Our data suggest that the initial step in the formation of acetaldehyde is the cleavage of the carbon-hydrogen bond of the methane molecule,



The experimental enthalpy for this reaction is that it is endoergic (energetically unfavorable) by 439 kJ mol^{-1} (4.5 eV). Our experiment indicates that each electron generates 28 ± 18 methyl radicals within the ice (§ 5.2.2); therefore, an energy transfer of 126 eV per implant is necessary to account for the spectroscopically observed column density of the methyl radical. Since the electron is being absorbed in our sample, 5 keV are available; this means that about 2.5% of the kinetic energy of each impinging electron is used to generate reactive methyl radicals and hydrogen atoms via equation (1). This calculation assumes that all the methyl radicals are formed in their vibrational ground states; in addition, the hydrogen atoms have no excess translational energy. However, to escape the matrix cage, each hydrogen atom must have at least 0.5 eV excess kinetic energy; if its kinetic energy is less than the lattice bonding energy, the hydrogen atom will react back with the methyl radical to regenerate a methane molecule. To fit the experimentally obtained methane column density, we assumed that the methane molecule undergoes first-order “decay” upon electron bombardment, similar to a radioactive decay. Therefore, a velocity law,

$$-d[CH_4]/dt = k_1[CH_4], \quad (2)$$

was used to fit the column density of the methane molecule during the irradiation phase via

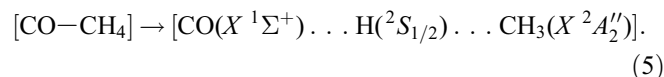
$$[CH_4](t) = [CH_4](t=0)e^{k_1 t}. \quad (3)$$

In a similar manner, the column density of carbon monoxide follows

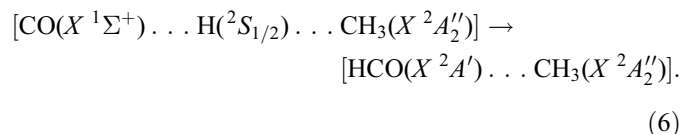
$$[CO](t) = [CO](t=0)e^{k_2 t}. \quad (4)$$

The best fit of the methane profile yields $[CH_4](t=0) = (5.46 \pm 0.04) \times 10^{17} \text{ cm}^{-2}$ and $k_1 = (8.35 \pm 6.81) \times 10^{-6} \text{ s}^{-1}$. It is actually very difficult to fit the decay of the carbon monoxide column density, simply because our experimental conditions were chosen so that less than 1% of the species were destroyed by the electrons. This condition guarantees nonoverlapping cascades and trajectories, which would not occur in the interstellar medium. Here, we find that $[CO](t=0) = (2.93 \pm 0.02) \times 10^{18} \text{ cm}^{-2}$; the k_2 constant has, because of the reasons described above, large uncertainties and is on the order of a few times 10^{-6} s^{-1} .

What is the fate of the generated hydrogen atoms and methyl radicals? We were able to fit the temporal evolution of the methyl and formyl radicals as well as of the acetaldehyde molecule with the following scenario (Fig. 9). Considering a $[CO-CH_4]$ van der Waals complex in the solid, the carbon-hydrogen bond cleavage releases a hydrogen atom to form a methyl radical and a hydrogen atom in the matrix cage:



Because of energy and angular momentum conservation, the hydrogen atom holds an excess kinetic energy (suprathreshold hydrogen atoms), which can be used either to escape from the matrix cage or to overcome the barrier to add to the carbon monoxide molecule (11 kJ mol^{-1} [0.12 eV]), forming the formyl radical within the matrix cage:



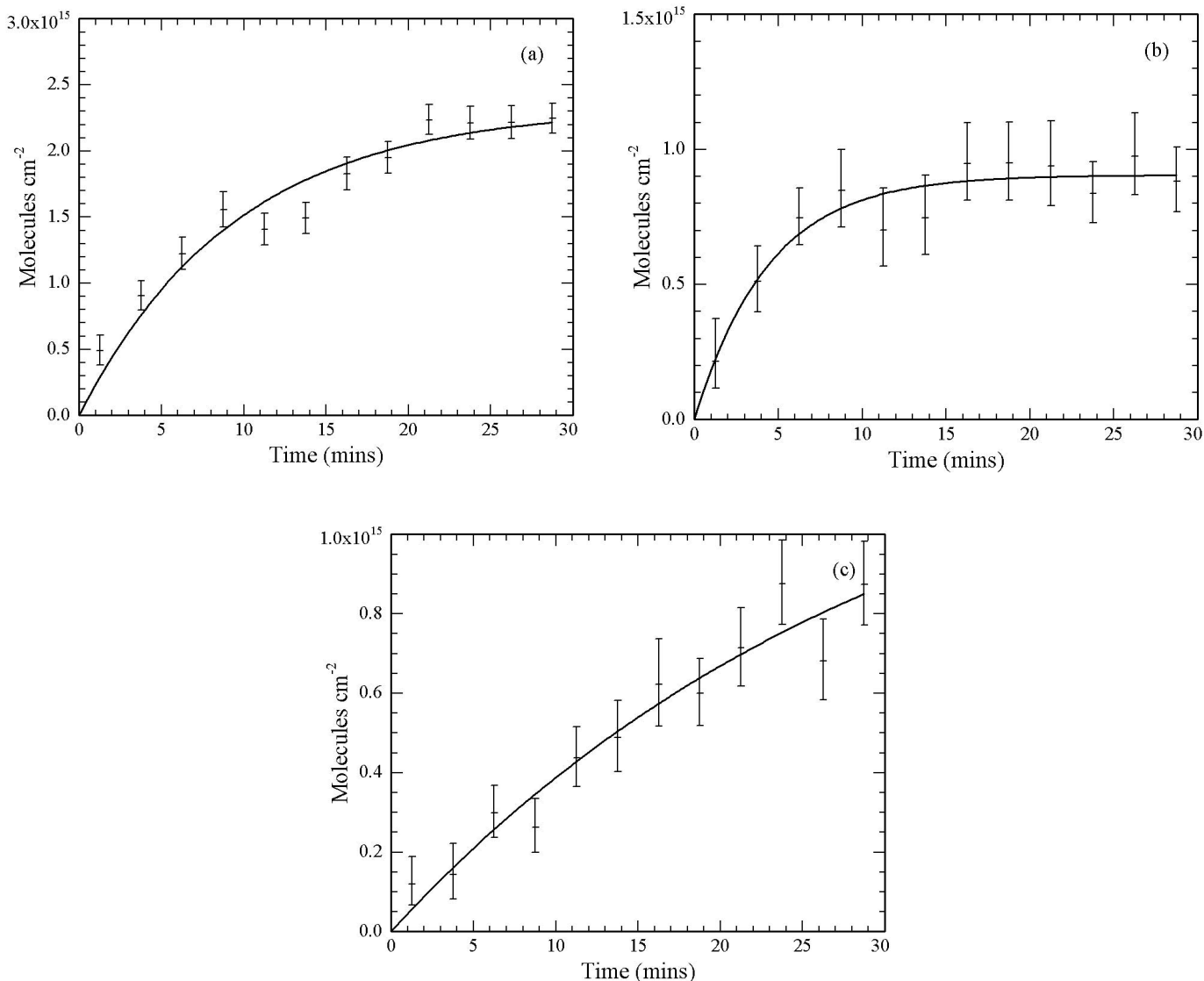


FIG. 9.— Column densities and fits of (a) the methyl radical at 612 cm⁻¹, (b) the formyl radical averaged from peaks at 1090 and 1853 cm⁻¹, and (c) the acetaldehyde molecule at 1728 cm⁻¹ during irradiation using eqs. (7), (8), and (11), respectively.

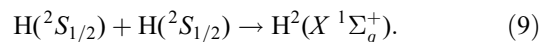
This mechanism would be first order with respect to the appearances of the methyl and the formyl radicals. In addition, we would expect a methyl radical to formyl radical ratio of 1:1, if each released hydrogen atom reacted with a carbon monoxide molecule to the formyl radical species. Therefore, we used

$$[\text{CH}_3](t) = a(1 - e^{-k_3 t}), \quad (7)$$

$$[\text{HCO}](t) = b(1 - e^{-k_4 t}), \quad (8)$$

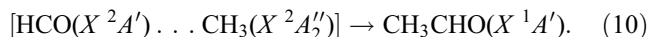
as derived from first-order rate laws, to fit the column densities of (1) the methyl radical and (2) the *pseudo*-first-order rate law of the formyl radical with the rate constants of the formation of the formyl and methyl radicals, k_3 and k_4 , respectively. This procedure yields rate constants of $k_3 = (1.75 \pm 0.28) \times 10^{-3}$ and $k_4 = (3.80 \pm 0.60) \times 10^{-3}$ s⁻¹ as well as a and b values of $(2.33 \pm 0.14) \times 10^{15}$ and $(9.05 \pm 0.31) \times 10^{14}$ cm⁻², respectively. It is important to stress that the rate constant to form the formyl radical is larger than that for the generation of the methyl radical (Figs. 9a and 9b). This is indicative of a reaction of *suprathermal hydrogen atoms* (which are not in thermal equilib-

rium with the surrounding 10 K matrix), released and reacted via equations (5) and (6). However, it should be noted that we are generating more methyl radicals than formyl radicals; comparison of the a and b values suggests that as $t \rightarrow \infty$, only about 39% of the suprathermal hydrogen atoms formed from the destruction of methane go on to form formyl radicals. This leads to the conclusion that not every suprathermal hydrogen atom reacts with a neighboring carbon monoxide molecule within the matrix cage to form the formyl radical species; for example, it can escape the matrix cage, thermalize, and/or react with a second hydrogen atom to form molecular hydrogen via



These considerations help us to understand the experimental observation of the methyl and formyl radicals as well as of the molecular hydrogen as detected via the quadrupole mass spectrometer. However, how can this model account for the synthesis of acetaldehyde? We have to keep in mind that the methyl radical and the formyl radical do not diffuse at 10 K. Therefore, the barrierless recombination of formyl and methyl radicals can only be

between neighboring radical species generated in a matrix cage via



If the rate constant for reaction (10) is much faster than those derived from the synthesis of the methyl and formyl radicals, then the temporal evolution of acetaldehyde can also be fitted with a pseudo-first-order reaction,

$$[\text{CH}_3\text{CHO}](t) = c(1 - e^{-kst}). \quad (11)$$

This mechanism requires that each methyl and formyl radical reaction via equations (5) and (6) have the appropriate geometry in the matrix cage that allows both radical centers to recombine. If the geometry criterion is not fulfilled, the reaction stops with equation (6), and formation of acetaldehyde cannot take place. Using equation (11) to fit the experimental data (Fig. 9c) yields $k_5 = (5.36 \pm 2.28) \times 10^{-4} \text{ s}^{-1}$ and $c = (1.41 \pm 0.42) \times 10^{15} \text{ cm}^{-2}$.

Recall that the overall reaction energy to form acetaldehyde from the methane and carbon monoxide reactants is experimentally determined to be endoergic by about 15 kJ mol⁻¹ (Table 3). Therefore, thermal reactants cannot form acetaldehyde in the low-temperature ices, as present on interstellar grains and in our solar system. An external energy source such as energetic cosmic-ray particles triggering δ -electrons is clearly required to compensate for the endoergic nature of the reaction and to generate suprathreshold hydrogen atoms, which can overcome the barrier for addition to the carbon-oxygen triple bond of the carbon monoxide molecule. These considerations underline the role of nonequilibrium (suprathreshold) chemistry in the formation of organic molecules in extraterrestrial ices.

Finally, we would like to address briefly the failed detection/formation of the HOC(*X*²*A'*), CH₃CO(*X*²*A'*), and CH₃OC(*X*²*A'*) radicals. Considering the reaction of a hydrogen atom with the carbon monoxide molecule, the formation of the formyl radical, HCO(*X*²*A'*), is exoergic and requires passing a lower entrance barrier of only 11 kJ mol⁻¹, compared to 139 kJ mol⁻¹ for the production of the isoformyl species, HOC(*X*²*A'*) (Fig. 4). Therefore, our data suggest that suprathreshold hydrogen atoms can easily pass TS1, but not TS2. This could put an upper limit of the energies of the suprathreshold hydrogen atoms to less than 1.4 eV (139 kJ mol⁻¹). The enhanced reactivity of the carbon center is due to the fact that the lowest unoccupied molecular orbital (LUMO) of the carbon monoxide molecule, with which the 1s orbital of the reacting hydrogen atom overlaps, has a larger overlap integral coefficient with the wave function at the carbon atom compared to the oxygen atom. This would explain the formation of the formyl radical instead of the isoformyl species. Likewise, the barriers involved in the formation of CH₃CO(*X*²*A'*) and CH₃OC(*X*²*A'*) are located higher in energy than TS1. This situation becomes even more interesting, as the methyl radical actually has no excess kinetic energy to overcome the barrier (the methyl radicals cannot diffuse in 10 K ices). After the initial carbon-hydrogen bond rupture, they can be formed with an excess vibrational energy. Since, however, both the formation of HCO(*X*²*A'*) and that of CH₃CO(*X*²*A'*) are exothermic and both transition states TS1 and TS3 are “early” (reactant-like), kinetic energy (such as from the suprathreshold hydrogen atom) is much more effective to overcome any barrier than vibrational excitation (such as the methyl radical; Levine & Bernstein 1987). In addition, the vibrational excitation can be coupled with the surrounding matrix and generate phonons, thus thermalizing the initially formed nonequilibrium vibration population of the

methyl radicals. Therefore, the dynamics and kinetics of the reaction favor the addition of the hydrogen atom to the carbon monoxide molecule followed by a barrierless recombination with the methyl radical in the matrix cage; a dominating route through any CH₃CO(*X*²*A'*) can likely be ruled out similarly to the one-step pathway via TSa and TSb (Fig. 4).

7. ASTROPHYSICAL IMPLICATIONS

Our combined experimental and theoretical studies provided detailed data on the formation of acetaldehyde in interstellar ices. The specific identification of acetaldehyde in low-temperature (10 K) carbon monoxide–methane ices suggested that cosmic particle-generated δ -electrons can initiate a carbon-hydrogen bond rupture process in the methane molecule, CH₄(*X*¹*A*₁), to form a methyl radical, CH₃(*X*²*A*₂''), and a hydrogen atom. The latter holds an excess kinetic energy and therefore is not in thermal equilibrium with the surrounding 10 K matrix; the excess kinetic energy can be imparted into the transition state of the addition of a hydrogen atom to the carbon monoxide molecule to give the formyl radical, HCO(*X*²*A'*). If the formyl and the methyl radical have the correct orientation, both species can undergo a barrierless radical-radical recombination within the matrix cage to synthesize the acetaldehyde molecule, CH₃CHO(*X*¹*A'*). The overall reaction to form acetaldehyde from the reactants is endoergic by 15 kJ mol⁻¹; this emphasizes the crucial role of nonequilibrium chemistry and the involvement of suprathreshold hydrogen atoms. Once acetaldehyde has been generated on ice-coated grains in cold molecular clouds, those molecules can sublime as soon as the cloud reaches the hot molecular core stage. These studies can account for the “missing” source of acetaldehyde in star-forming regions such as Sgr B2, which have high fractional abundances of acetaldehyde of a few times 10⁻⁹ (Nummelin et al. 1998; Ikeda et al. 2001; Chengalur & Kanekar 2003; Chamley 2004), compared to abundances of only some 10⁻¹⁰ in the cold cloud TMC-1, where solely gas-phase reactions are supposed to form acetaldehyde. Our investigations also suggest that acetaldehyde might indeed be the carrier of the 1348 cm⁻¹ (7.414 μm ; CH deformation mode) band observed toward interstellar ices, as surveyed by Gibb et al. (2004), where abundances of $\sim 9\%$ (relative to water) have been reported for the high-mass YSOs W33A and AFGL 7009S, as well as a detectable presence of the band in 12 of the 23 sources surveyed. It is also quite credible that the same synthetic route could help explain the formation of acetaldehyde at 0.025% abundance (relative to water) in comet C/1995 O1 (Hale-Bopp) detected by Crovisier et al. (2004).

The present work is a first step to understanding the formation of acetaldehyde systematically. Future laboratory experiments should investigate how water additives, the dominating component of interstellar and cometary ices, will influence the reaction mechanism. First, we could expect a dilution of the reaction centers; however, in order to form acetaldehyde, the conclusions drawn in the present paper are still correct, i.e., that we need neighboring carbon monoxide–methane molecules to form the acetaldehyde via the recombination of the methyl with the formyl radical. Thus, it would also be important to investigate spectroscopically to what extent methane–carbon monoxide complexes remain in water-dominated ices. Finally, the water matrix can also influence the phonon coupling of the internally excited acetaldehyde molecule. This has to be investigated in future experiments, as well.

This work was supported by the Particle Physics and Astronomy Research Council (PPARC, UK; R. I. K.), the University of Hawaii at Manoa (C. J. B., C. S. J., R. I. K.), and by the

UH-NASA-Astrobiology Institute (C. J. B., R. I. K.). The computations were carried out at the computer center of the Institute for Molecular Science, Japan, and supported by the Grants-in-Aid for Scientific Research on Priority Areas from the Ministry

of Education, Science, and Culture, Japan (Y. O.). We are also grateful to Ed Kawamura and Dave Kempton (both at the University of Hawaii, Department of Chemistry) for their electrical and mechanical work.

APPENDIX

In order to correctly identify and quantify the new species produced during our experiment via infrared spectroscopy, it is necessary to carry out theoretical electronic structure calculations to give us information about the frequencies at which these molecules will appear (given in cm^{-1} and μm) and how strong these absorptions should be (cm molecule^{-1}). Although some information already exists regarding some of these data (both theoretical and experimental), it is prudent to use frequencies and intensities all derived from the same level of theory to avoid unnecessary complications and errors that may arise from combining the assortment of information already available. The vibrational frequencies and infrared intensities shown here (Table A1) were calculated from structures obtained from using the hybrid density functional B3LYP method (Lee et al. 1988; Becke 1993) with the 6-311G(d,p) basis functions. The scaling factor of 0.98 is an average value derived from comparison of the calculated vibrational frequencies to the experimental frequencies (where available) and is consistent for this level of theory. The accuracy of the infrared intensities is accurate within 20% at this level of theory (Galabov et al. 2002).

TABLE A1
CALCULATED VIBRATIONAL FREQUENCIES AND INTEGRAL ABSORPTION COEFFICIENTS OF VARIOUS SPECIES

Band	Characterization	Band Position [cm^{-1} (μm)]	A (cm molecule^{-1})
CO ($X^1\Sigma^+$)			
ν_1 (Σ^+)	Stretching	2176 (4.60)	1.26×10^{-17}
CH ₄ (X^1A_1)			
ν_1 (a_1)	CH stretching	2965 (3.37)	0
ν_2 (e)	Bending	1530 (6.54)	1.66×10^{-19}
ν_3 (t)	CH stretching	3068 (3.26)	4.65×10^{-18}
ν_4 (t)	Bending	1315 (7.60)	2.82×10^{-18}
CH ₃ (X^2A_2'')			
ν_1 (a_1')	CH stretching	3042 (3.29)	0
ν_2 (a_2'')	Out of plane	496 (20.17)	1.39×10^{-17}
ν_3 (e')	CH stretching	3217 (3.11)	1.16×10^{-18}
ν_4 (e')	Bending	1376 (7.27)	6.64×10^{-19}
HCO (X^2A')			
ν_1 (a')	CH stretching	2568 (3.90)	1.56×10^{-17}
ν_2 (a')	CO stretching	1902 (5.26)	1.48×10^{-17}
ν_3 (a')	Bending	1089 (9.19)	6.64×10^{-18}
HOC (X^2A')			
ν_1 (a')	OH stretching	3200 (3.13)	1.06×10^{-17}
ν_2 (a')	CO stretching	1360 (7.35)	6.14×10^{-18}
ν_3 (a')	Bending	1108 (9.02)	1.36×10^{-17}
CH ₃ CO (X^2A')			
ν_1 (a')	CH ₃ asymmetric stretching	3047 (3.28)	1.83×10^{-18}
ν_2 (a')	CH ₃ symmetric stretching	2957 (3.38)	1.83×10^{-18}
ν_3 (a')	CO stretching	1893 (5.28)	2.51×10^{-17}
ν_4 (a')	CH ₃ deformation	1428 (7.00)	3.65×10^{-18}
ν_5 (a')	CH ₃ umbrella	1326 (7.54)	2.66×10^{-18}
ν_6 (a')	CH ₃ rocking	1024 (9.77)	2.49×10^{-18}
ν_7 (a')	CC stretching	829 (12.06)	9.96×10^{-19}
ν_8 (a')	CCO bending	458 (21.85)	8.30×10^{-19}
ν_9 (a'')	CH ₃ asymmetric stretching	3052 (3.23)	4.98×10^{-19}
ν_{10} (a'')	CH ₃ deformation	1425 (7.02)	2.32×10^{-18}
ν_{11} (a'')	CH ₃ twisting	933 (10.72)	0
ν_{12} (a'')	Torsion	107 (93.62)	1.66×10^{-19}

TABLE A1—Continued

Band	Characterization	Band Position [cm ⁻¹ (μ m)]	<i>A</i> (cm molecule ⁻¹)
CH ₃ OC (<i>X</i> ² <i>A'</i>)			
ν_1 (<i>a'</i>).....	CH ₃ asymmetric stretching	3112 (3.21)	9.96×10^{-19}
ν_2 (<i>a'</i>).....	CH ₃ symmetric stretching	2998 (3.34)	1.99×10^{-18}
ν_3 (<i>a'</i>).....	OC stretching, CH ₂ bending	1455 (6.87)	5.31×10^{-18}
ν_4 (<i>a'</i>).....	CH ₃ deformation	1441 (6.94)	0
ν_5 (<i>a'</i>).....	CH ₃ umbrella	1311 (7.63)	5.65×10^{-18}
ν_6 (<i>a'</i>).....	CH ₃ rocking	1094 (9.14)	0
ν_7 (<i>a'</i>).....	CH ₃ -O stretching	570 (17.53)	3.32×10^{-19}
ν_8 (<i>a'</i>).....	COC bending	429 (23.30)	9.96×10^{-19}
ν_9 (<i>a''</i>).....	CH ₃ asymmetric stretching	3117 (3.21)	1.66×10^{-18}
ν_{10} (<i>a''</i>).....	CH ₃ deformation	1444 (6.93)	1.16×10^{-18}
ν_{11} (<i>a''</i>).....	CH ₃ twisting	1058 (9.45)	1.66×10^{-19}
ν_{12} (<i>a''</i>).....	Torsion	125 (79.72)	0
CH ₃ CHO (<i>X</i> ¹ <i>A'</i>)			
ν_1 (<i>a'</i>).....	CH ₃ asymmetric stretching	3073 (3.25)	1.99×10^{-18}
ν_2 (<i>a'</i>).....	CH ₃ symmetric stretching	2961 (3.38)	4.98×10^{-19}
ν_3 (<i>a'</i>).....	CH stretching	2798 (3.57)	2.41×10^{-17}
ν_4 (<i>a'</i>).....	CO stretching	1788 (5.59)	2.97×10^{-17}
ν_5 (<i>a'</i>).....	CH ₃ deformation	1431 (6.99)	3.65×10^{-18}
ν_6 (<i>a'</i>).....	CH bending	1397 (7.16)	1.99×10^{-18}
ν_7 (<i>a'</i>).....	CH ₃ umbrella	1348 (7.42)	4.48×10^{-18}
ν_8 (<i>a'</i>).....	CH ₃ rocking	1103 (9.06)	4.32×10^{-18}
ν_9 (<i>a'</i>).....	C-C stretching	865 (11.56)	1.49×10^{-18}
ν_{10} (<i>a'</i>).....	CCO bending	498 (20.09)	2.32×10^{-18}
ν_{11} (<i>a''</i>).....	CH ₃ asymmetric stretching	3014 (3.32)	1.66×10^{-18}
ν_{12} (<i>a''</i>).....	CH ₃ deformation	1442 (6.94)	1.99×10^{-18}
ν_{13} (<i>a''</i>).....	HCCH torsion	1112 (8.99)	1.66×10^{-19}
ν_{14} (<i>a''</i>).....	CH ₃ twisting	761 (13.13)	1.66×10^{-19}
ν_{15} (<i>a''</i>).....	CH ₃ torsion	156 (64.18)	0
TS1 H-CO (<i>X</i> ² <i>A'</i>)			
ν_1 (<i>a'</i>).....	CO stretching	2146 (4.66)	2.03×10^{-17}
ν_2 (<i>a'</i>).....	Bending	252 (39.71)	1.66×10^{-19}
ν_3 (<i>a'</i>).....	H-C stretching	394 (25.38) <i>i</i>	3.32×10^{-19}
TS2 H-OC (<i>X</i> ² <i>A'</i>)			
ν_1 (<i>a'</i>).....	CO stretching	1799 (5.56)	7.80×10^{-18}
ν_2 (<i>a'</i>).....	Bending	972 (10.29)	2.99×10^{-18}
ν_3 (<i>a'</i>).....	H-O stretching	1816 (5.51) <i>i</i>	4.81×10^{-16}
TS3 CH ₃ -CO (<i>X</i> ² <i>A'</i>)			
ν_1 (<i>a'</i>).....	CH ₃ asymmetric stretching	3208 (3.12)	6.64×10^{-19}
ν_2 (<i>a'</i>).....	CH ₃ symmetric stretching	3033 (3.30)	0
ν_3 (<i>a'</i>).....	CO stretching	2058 (4.86)	4.43×10^{-17}
ν_4 (<i>a'</i>).....	CH ₃ bending	1382 (7.24)	6.64×10^{-19}
ν_5 (<i>a'</i>).....	CH ₃ umbrella	804 (12.44)	5.15×10^{-18}
ν_6 (<i>a'</i>).....	CH ₃ rocking	501 (19.97)	0
ν_7 (<i>a'</i>).....	C...CO bending	237 (42.17)	1.66×10^{-19}
ν_8 (<i>a'</i>).....	C...C stretching	271 (36.84) <i>i</i>	8.30×10^{-19}
ν_9 (<i>a''</i>).....	CH ₃ asymmetric stretching	3193 (3.13)	6.64×10^{-19}
ν_{10} (<i>a''</i>).....	CH ₃ deformation	1388 (7.21)	8.30×10^{-19}
ν_{11} (<i>a''</i>).....	CH ₃ twisting	458 (21.85)	0
ν_{12} (<i>a''</i>).....	Torsion	15 (680.27)	0

TABLE A1—Continued

Band	Characterization	Band Position [cm ⁻¹ (μ m)]	<i>A</i> (cm molecule ⁻¹)
TS4 CH ₃ —OC (<i>X</i> ² <i>A'</i>)			
ν_1 (<i>a'</i>).....	CH ₃ asymmetric stretching	3142 (3.18)	8.30×10^{-19}
ν_2 (<i>a'</i>).....	CH ₃ symmetric stretching	3009 (3.32)	4.98×10^{-19}
ν_3 (<i>a'</i>).....	OC stretching	1448 (6.90)	8.80×10^{-18}
ν_4 (<i>a'</i>).....	CH ₃ deformation	1429 (7.00)	1.66×10^{-18}
ν_5 (<i>a'</i>).....	CH ₃ umbrella	1260 (7.94)	3.15×10^{-18}
ν_6 (<i>a'</i>).....	CH ₃ rocking	1005 (9.95)	6.64×10^{-19}
ν_7 (<i>a'</i>).....	C...OC bending	444 (22.53)	1.83×10^{-18}
ν_8 (<i>a'</i>).....	CH ₃ ...O stretching	518 (19.29) <i>i</i>	1.99×10^{-17}
ν_9 (<i>a''</i>).....	CH ₃ asymmetric stretching	3148 (3.18)	1.16×10^{-18}
ν_{10} (<i>a''</i>).....	CH ₃ deformation	1429 (7.00)	9.96×10^{-19}
ν_{11} (<i>a''</i>).....	CH ₃ twisting	953 (10.50)	1.66×10^{-19}
ν_{12} (<i>a''</i>).....	Torsion	104 (96.27)	0

NOTES.—Included species are reactants, potential intermediates, products, various transition states (see Fig. 4), and expected molecules produced from the destruction of acetaldehyde calculated with the B3LYP/6-311G(d,p) method. The frequencies have been scaled by a factor of 0.98 (see text for details).

REFERENCES

- Allamandola, L. J., Bernstein, M. P., Sandford, S. A., & Walker, R. L. 1999, *Space Sci. Rev.*, 90, 219
- Alsindi, W. Z., Gardner, D. O., van Dishoeck, E. F., & Fraser, H. J. 2003, *Chem Phys. Lett.*, 378, 178
- Baratta, G. A., Leto, G., & Palumbo, M. E. 2002, *A&A*, 384, 343
- Becke, A. D. 1993, *J. Chem. Phys.*, 98, 5648
- Belbruno, J. J. 1997, *J. Phys. Organic Chem.*, 10, 113
- Bell, M. B., Mathews, H. E., & Feldman, P. A. 1983, *A&A*, 127, 420
- Bennett, C. J., Jamieson, C., Mebel, A. M., & Kaiser, R. I. 2004, *Phys. Chem. Chem. Phys.*, 6, 735
- Bernstein, M. P., Dworkin, J. P., Sandford, S. A., Cooper, G. W., & Allamandola, L. J. 2002, *Nature*, 416, 401
- Biver, N., et al. 2002, *Earth Moon Planets*, 90, 323
- Boogert, A. C. A., Helmich, F. P., van Dishoeck, E. F., Schutte, W. A., Tielens, A. G. G. M., & Whittet, D. C. B. 1998, *A&A*, 336, 352
- Boogert, A. C. A., Schutte, W. A., Helmich, F. P., Tielens, A. G. G. M., & Wooden, D. H. 1997, *A&A*, 317, 929
- Boogert, A. C. A., et al. 1996, *A&A*, 315, L377
- Brucato, J. R., Palumbo, M. E., & Strazzulla, G. 1997, *Icarus*, 125, 135
- Charnley, S. B. 2004, *Adv. Space Res.*, 33, 23
- Chengalur, J. N., & Kanekar, N. 2003, *A&A*, 403, L43
- Crovisier, J. 1998, *Faraday Discuss.*, 109, 437
- Crovisier, J., Bockelée-Morvan, D., Colom, P., Biver, N., & Despois, D. 2004, *A&A*, 418, 1141
- Curtiss, L. A., Raghavachari, K., Redfern, P. C., Rassolov, V., & Pople, J. A. 1998, *J. Chem. Phys.*, 109, 7764
- Curtiss, L. A., Raghavachari, K., Trucks, G. W., & Pople, J. A. 1991, *J. Chem. Phys.*, 94, 7221
- Dartois, E., Demyk, K., d'Hendecourt, L., & Ehrenfreund, P. 1999, *A&A*, 351, 1066
- Diau, E. W.-G., Kötting, C., Sølling, T. I., & Zewail, A. H. 2002, *Chem-PhysChem*, 3, 57
- Dickens, J. E., Irvine, W. M., Ohishi, M., Ikeda, M., Ishikawa, S., Nummelin, A., & Hjalmarsen, A. 1997, *ApJ*, 489, 753
- Drouin, D., Couture, A. R., Gauvin, R., Hovington, P., Horny, P., & Demers, H. 2001, Monte Carlo Simulation of Electron Trajectory in Solids (CASINO) (ver. 2.42; Sherbrooke: Univ. Sherbrooke)
- Dunning, T. H. 1989, *J. Chem. Phys.*, 90, 1007
- Ehrenfreund, P., Boogert, A. C. A., Gerakines, P. A., Jansen, D. J., Schutte, W. A., Tielens, A. G. G. M., & van Dishoeck, E. F. 1996, *A&A*, 312, 263
- Ehrenfreund, P., d'Hendecourt, L., Dartois, E., Jourdain de Muizon, M., Breitfellner, M., Puget, J. L., & Habing, H. J. 1997, *Icarus*, 130, 1
- Ehrenfreund, P., & Schutte, W. A. 2000, in *IAU Symp. 197, Astrochemistry: From Molecular Clouds to Planetary Systems*, ed. Y. C. Minh & E. F. van Dishoeck (San Francisco: ASP), 135
- El-Nawawy, M. S., Howe, D. A., & Millar, T. J. 1997, *MNRAS*, 292, 481
- Ewing, G. E., Thompson, W. E., & Pimentel, G. C. 1960, *J. Chem. Phys.*, 32, 927
- Fairley, D. A., Scott, G. B. I., Freeman, C. G., MacLagan, R. G. A. R., & McEwan, M. J. 1996, *J. Chem. Soc. Faraday Trans.*, 92, 1305
- Fourikis, N., Sinclair, M. W., Robinson, B. J., Godfrey, P. D., & Brown, R. D. 1974, *Australian J. Phys.*, 27, 425
- Fraser, H. J., McCoustra, M. R. S., & Williams, D. A. 2002, *Astron. Geophys.*, 43(2), 10
- Frisch, M. J., et al. 2001, *Gaussian 98* (Rev. A.9; Pittsburgh: Gaussian, Inc.)
- Galabov, B., Yamaguchi, Y., Remington, R. B., & Schaefer, H. F., III. 2002, *J. Phys. Chem. A*, 106, 819
- Gerakines, P. A., Moore, M. H., & Hudson, R. L. 2004, *Icarus*, 170, 202
- Gerakines, P. A., Schutte, W. A., & Ehrenfreund, P. 1996, *A&A*, 312, 289
- Gerakines, P. A., Schutte, W. A., Greenberg, J. M., & van Dishoeck, E. F. 1995, *A&A*, 296, 810
- Gibb, E. L., Nummelin, A., Irvine, W. M., Whittet, D. C. B., & Bergman, P. 2000, *ApJ*, 545, 309
- Gibb, E. L., Whittet, D. C. B., Boogert, A. C. A., & Tielens, A. G. G. M. 2004, *ApJS*, 151, 35
- Hawkins, M., & Andrews, L. 1983, *J. Am. Chem. Soc.*, 105, 9
- Hjalmarsen, A., Bergman, P., & Nummelin, A. 2001, in *Proc. 1st European Workshop on Exo-/astro-biology*, ed. P. Ehrenfreund, O. Angerer, & B. Battrick (ESA SP-496; Noordwijk: ESA), 263
- Hudson, R. L., & Moore, M. H. 1999, *Icarus*, 140, 451
- Ikeda, M., Ohishi, M., Nummelin, A., Dickens, J. E., Bergman, P., Hjalmarsen, A., & Irvine, W. M. 2001, *ApJ*, 560, 792
- Jacox, M. E. 1982, *Chem. Phys.*, 69, 407
- Jamieson, C. S., Bennett, C. J., & Kaiser, R. I. 2005, *ApJ*, 624, 436
- Johnson, R. E. 1990, *Energetic Charged Particle Interactions with Atmospheres and Surfaces* (Berlin: Springer)
- . 1996, *Rev. Mod. Phys.*, 68, 305
- Jursic, B. S. 1998, *J. Mol. Struct.*, 427, 157
- Kaiser, R. I. 2002, *Chem. Rev.*, 102, 1309
- Kaiser, R. I., Eich, G., Gabrysch, A., & Roessler, K. 1997, *ApJ*, 484, 487
- . 1999, *A&A*, 346, 340
- Kaiser, R. I., & Roessler, K. 1997, *ApJ*, 475, 144
- . 1998, *ApJ*, 503, 959
- Keane, J. V., Tielens, A. G. G. M., Boogert, A. C. A., Schutte, W. A., & Whittet, D. C. B. 2001, *A&A*, 376, 254
- Keller, H.-M., Floethmann, H., Dobbyn, A. J., Schinke, R., Werner, H.-J., Bausier, C., & Rosmus, P. 1996, *J. Chem. Phys.*, 105, 4983
- Krupskii, I. N., Prokhvatilov, A. I., Erenburg, A. I., & Yantsevich, L. D. 1973, *Phys. Status Solidi A*, 19, 519
- Kurosaki, Y., & Yokoyama, K. 2003, *Chem. Phys. Lett.*, 371, 568
- Lecluse, C., Robert, F., Kaiser, R. I., Roessler, K., Pillinger, C. T., & Javoy, M. 1998, *A&A*, 330, 1175
- Lee, C., Yang, W., & Parr, R. G. 1988, *Phys. Rev. B*, 37, 785
- Levine, R. D., & Bernstein, R. B. 1987, *Molecular Reaction Dynamics and Chemical Reactivity* (Oxford: Oxford Univ. Press)
- Mathews, H. E., Friberg, P., & Irvine, W. M. 1985, *ApJ*, 290, 609
- Millar, T. J., & Hatchell, J. 1998, *Faraday Discuss.*, 109, 15
- Millar, T. J., Herbst, E., & Charnley, S. B. 1991, *ApJ*, 369, 147
- Millar, T. J., MacDonald, G. H., & Gibb, A. G. 1997, *A&A*, 325, 1163

- Milligan, D. E., & Jacox, M. E. 1964, *J. Chem. Phys.*, 41, 3032
———. 1967, *J. Chem. Phys.*, 47, 5146
———. 1969, *J. Chem. Phys.*, 51, 277
- Minh, Y. C., & van Dishoeck, E. F., eds. 2000, *IAU Symp. 197, Astrochemistry: From Molecular Clouds to Planetary Systems* (San Francisco: ASP)
- Moore, M. H., & Hudson, R. L. 1998, *Icarus*, 135, 518
———. 2003, *Icarus*, 161, 486
- Mordaunt, D. H., Ashfold, M. N. R., Dixon, R. N., Loffler, P., Schnieder, L., & Welge, K. H. 1998, *J. Chem. Phys.*, 108, 519
- Muñoz Caro, G. M., & Schutte, W. A. 2003, *A&A*, 412, 121
- North, S., Blank, D. A., & Lee, Y. T. 1994, *Chem Phys. Lett.*, 224, 38
- Nummelin, A., Dickens, J. E., Bergman, P., Hjalmarsen, A., Irvine, W. M., Ikeda, M., & Ohishi, M. 1998, *A&A*, 337, 275
- Palumbo, M. E., Castorina, A. C., & Strazzulla, G. 1999, *A&A*, 342, 551
- Palumbo, M. E., Pendleton, Y. J., & Strazzulla, G. 2000, *ApJ*, 542, 890
- Pettersson, M., Khriachtchev, L., Jolkkonen, S., & Raesaenen, M. 1999, *J. Phys. Chem. A*, 103, 9154
- Prasad, S. S., & Tarafdar, S. P. 1983, *ApJ*, 267, 603
- Purvis, G. D., & Bartlett, R. J. 1982, *J. Chem. Phys.*, 76, 1910
- Raghavachari, K., Trucks, G. W., Pople, J. A., & Head-Gordon, M. 1989, *Chem. Phys. Lett.*, 157, 479
- Roessler, K. 1992, *Nucl. Instrum. Methods Phys. Res. B*, 65, 55
- Ruffle, D. P., & Herbst, E. 2001, *MNRAS*, 322, 770
- Sandford, S. A., Allamandola, L. J., Tielens, A. G. G. M., & Valero, G. J. 1988, *ApJ*, 329, 498
- Schriver, A., Coanga, J. M., Shriver-Mazzouli, L., & Ehrenfreund, P. 2004, *Chem. Phys.*, 303, 13
- Schutte, W. A. 1999, in *Laboratory Astrophysics and Space Research*, ed. P. Ehrenfreund et al. (Dordrecht: Kluwer), 69
———. 2002, *Adv. Space Res.*, 30, 1409
- Schutte, W. A., et al. 1999, *A&A*, 343, 966
- Shimanouchi, T. 1972, *Tables of Molecular Vibrational Frequencies Consolidated, Vol. I* (NSRDS-NBs 39; Washington: National Bureau of Standards)
- Smith, B. J., Nguyen, M. T., Bouma, W. J., & Radom, L. 1991, *J. Am. Chem. Soc.*, 113, 6452
- Smith, R. 1997, *Atomic and Ion Collisions in Solids and at Surfaces* (Cambridge: Cambridge Univ. Press)
- Snelson, A. 1970, *J. Phys. Chem.*, 74, 537
- Stäuber, P., Doty, S. D., van Dishoeck, E. F., Jørgensen, J. K., & Benz, A. O. 2004, *A&A*, 425, 577
- Strazzulla, G., & Johnson, R. E. 1991, in *Comets in the Post-Halley Era*, ed. R. L. Newburn, Jr., M. Neugebauer, & J. Rahe (Dordrecht: Kluwer), 243
- Strazzulla, G., & Palumbo, M. E. 1998, *Planet. Space Sci.*, 46, 1339
- Tielens, A. G. G. M., & Allamandola, L. J. 1987, in *Interstellar Processes*, ed. D. J. Hollenbach & H. A. Thronson (Dordrecht: Reidel), 397
- Tielens, A. G. G. M., & Hagen, W. 1982, *A&A*, 114, 245
- Tielens, A. G. G. M., Tokinaga, A. T., Geballe, T. R., & Baas, F. 1991, *ApJ*, 381, 181
- Turner, B. E. 1991, *ApJS*, 76, 617
- Turner, B. E., Terzieva, R., & Herbst, E. 1999, *ApJ*, 518, 699
- Wang, H. Y., Eyre, J. A., & Dorfman, L. M. 1973, *J. Chem. Phys.*, 59, 5199
- Werner, H.-J., Bauer, C., Rosmus, P., Keller, H.-M., Stumpf, M., & Schinke, R. 1995, *J. Chem. Phys.*, 102, 3593
- Wexler, A. S. 1967, *Appl. Spectrosc. Rev.*, 1, 29
- Woon, D. E. 1996, *J. Chem. Phys.*, 105, 9921
- Wyckoff, R. 1965, *Crystal Structures*, Vol. 4 (New York: Wiley)
- Yadav, J. S., & Goddard, J. D. 1986, *J. Chem. Phys.*, 84, 2682
- Ziurys, L. M., & McGonagle, D. 1993, *ApJS*, 89, 155
- Zou, Q., & Varanasi, P. 2002, *J. Quant. Spectrosc. Radiat. Transfer*, 75, 53